Large-scale deformation associated with ridge subduction

Eric L. Geist, Michael A. Fisher and David W. Scholl

US Geological Survey, 345 Middlefield Road, MS 999 Menlo Park, CA 94025, USA

SUMMARY

Continuum models are used to investigate the large-scale deformation associated with the subduction of aseismic ridges. Formulated in the horizontal plane using thin viscous sheet theory, these models measure the horizontal transmission of stress through the arc lithosphere accompanying ridge subduction. Modelling was used to compare the Tonga arc and Louisville ridge collision with the New Hebrides arc and d'Entrecasteaux ridge collision, which have disparate arc–ridge intersection speeds but otherwise similar characteristics. Models of both systems indicate that diffuse deformation (low values of the effective stress–strain exponent n) are required to explain the observed deformation. Deformation is somewhat insensitive to the vertically integrated strength of the arc (inversely proportional to the Argand number Ar), but indicates that the arc lithosphere is not extremely weak ($Ar < 100$). Low values of both Ar and n suggest that the thermal structure is typical of 'cold' or 'normal' arcs and that deformation is dominated by flow in the lower crust and mantle. In addition, low values of n (approaching Newtonian flow) may indicate that specific deformation mechanisms dictate deformation of the arc lithosphere. Possible mechanisms include low-stress, grain-size dependent creep, pyroxenite-controlled rheology and mechanisms associated with water weakening. Changes in the boundary conditions greatly affect deformation within island arcs. High rates of arc–ridge intersection speed (Tonga–Louisville system) yield arc-parallel tension and crustal thickening in the wake of ridge subduction. In contrast, low rates of arc–ridge intersection speed (New Hebrides–d'Entrecasteaux system) yield compressional deformation directly arcward of the collision zone and transverse strike–slip faulting adjacent to the region of compressional deformation. Localized regions of extensional deformation along the frontal part of the arc adjacent to the collision zone may contribute to the formation of re-entrants.

Key words: crustal deformation, island arcs, modelling, New Hebrides (Vanuatu), rheology, subduction, Tonga.

INTRODUCTION

Globally, many aseismic ridges on oceanic plates are actively being subducted. Many researchers have described corresponding changes in the dynamics of the subduction zone, including changes in deep and shallow seismicity and the morphology, deformation, accretion and volcanism of the upper plate. It is not possible to formulate a classification of these effects which can be applied to all subducting ridges, because at each collision zone, the structural and physiographic characteristics of the colliding structure and the margin differ, as does the speed and obliquity of subduction. The purpose of this study is to observe the effect that changes in the subduction parameters have on deformation associated with ridge subduction.

Previous investigations concerning the effects of ridge subduction on large-scale deformation of the arc have included both descriptive theories to explain observed structure and numerical modelling of the subduction process. Of the descriptive models, Moretti & Ngokwey (1985) and Bouysse & Westercamp (1990) have classified ridges as either buoyant or non-buoyant, based on whether the ridges are gravitationally compensated. By comparing the effects of both types of ridges on the Lesser Antilles arc, they note that the effects from subducting non-buoyant ridges are less, though still significant, than those from subducting buoyant ridges. Likewise, McCann & Habermann (1989) describe changes in the morphology, rate of accretion and type of forearc structures as they relate to the buoyancy and relief of the ridges world-wide.

The slip-line theory is from studies of perfectly plastic deformation and was used by Tapponier & Molnar (1976),

Collot, Daniel & Burne (1985) and Bouysse & Westercamp (1990) to explain faulting transverse to the trend of an impacted margin. Collot *et al.* (1985) and Bouysse & Westercamp (1990) model ridge subduction as a rigid die indenting a plastic medium, with deformation confined to the horizontal plane. However, England & McKenzie (1982) and Vilotte, Daignières & Madariaga (1982) note that the main limitation of plane horizontal strain modelling is that the horizontal principal deviatoric stresses must be equal and opposite so that only strike–slip faulting can be predicted. In addition, plane horizontal strain models do not take into account stresses arising from crustal thickness variations.

The numerical models of Chung & Kanamori (1978), Tomoda & Fujimoto (1983), Kodama (1984) and Moretti & Ngokwey (1985) calculate the vertical effects of ridge subduction. Chung & Kanamori (1978) assume that the subduction of the d'Entrecasteaux ridge acts as an upward load to uplift the frontal part of the New Hebrides arc and downwarp the region directly behind the uplift. For their calculations, the New Hebrides arc is modelled as as elastic plate overlying an inviscid fluid. Alternatively, Moretti & Ngokwey (1985) model the effects of ridge subduction at the Lesser Antilles arc using elastic and viscoelastic theory. They separate the process into two parts: (1) the collision process itself creating a bulge in the overriding plate from compression, and (3) isostatic adjustments originating from the anomalous density of the subducted ridge. They conclude that uplift adjacent to the collision zone is caused by the isostatic imbalance rather than from collision of the ridge at the plate boundary (see also Tomoda & Fujimoto 1983). Kodama (1984) models ridge subduction as a Newtonian viscous fluid overlying a rigid basement with harmonic undulations.

Few of the previous models consider the horizontal changes affecting the overriding plate caused by the local deviation of interplate stress due to ridge subduction. Collot *et al.* (1985) use an analogue of flexural bending of a beam in the horizontal plane to explain the extensional back-arc basins. For this analogy, the horizontal load causing flexure is the increased stress brought about by ridge subduction. However, the proposed existence of a peripheral bulge on an elastic beam would require an unexplained restoring force on the opposite side of the load, similar to the hydrostatic force necessary to explain the peripheral bulge associated with the load of island chains on an oceanic plate (Turcotte & Schubert 1982).

The objectives of this study are to model the large-scale effects of ridge subduction using continuum models and to note how deformation changes with different physical parameters. The ridge subduction process is simply considered as a local increase in interplate stress that depends on the arc–ridge intersection speed and rate of convergence (Fig. 1). These models are compared with previous models of vertical deformation to learn if most features associated with ridge subduction can be explained by the horizontal transmission of stress throughout an arc massif, or if vertical flexure plays a more important role in large-scale deformation. Also of interest is to estimate how far the effects of ridge subduction extend beyond the collision zone. In this way it is possible to test whether structures such as the back-arc basins of the New Hebrides

could have formed from ridge subduction, as proposed by Collot *et al.* (1985).

The principal boundary condition we use to model the ridge–arc interaction is the speed of the ridge–arc intersection. The intersection speed, in turn, depends on the convergence vector and the orientation of the ridge and arc (Fig. 1). We postulate that the arc–ridge intersection speed and rate of convergence of the ridge directly influence the style and magnitude of deformation. The Tonga–Louisville and New Hebrides–d'Entrecasteaux arc–ridge systems represent approximate end-members of the range of arc–ridge intersection speeds. These two arc–ridge systems lend themselves to comparison because other variables, such as the rate of convergence and the morphology of the subducting ridges, are similar. The intersection between the Louisville Ridge and the Tonga arc propagates southward at a fast rate of 180 km Myr^{-1} (Fig. 2; Ballance *et al.* 1989). In contrast, the intersection between the d'Entrecasteaux Ridge and the New Hebrides arc propagates slowly northward at a rate of 25 km Myr^{-1} (Fig. 3; Collot & Fisher 1991). Correspondingly, deformation of the two arcs that can be attributed to ridge subduction is noticeably different. The magnitude of deformation for other arcs or continental margins also depends on the rate of convergence, which can be much slower than for the two arcs studied here, although the style of deformation, which we are most concerned with, should be independent of the convergence rate.

Because the models in this study consider large-scale deformation only and do not take into account local changes in the relief of the ridge, smaller scale processes near the subduction zone, such as mass wasting and tectonic erosion, as described by Fryer & Smoot (1985), Fisher (1986), Fisher, Collot & Smith (1986), Lallemand & Le Pichon (1987), Burne, Collot & Daniel (1988), von Huene *et al.* (1988), Ballance *et al.* (1989), Collot & Fisher (1991), Fisher, Collot & Geist (1991) and Lallemand, Malavieille & Calassou (1992), are not addressed. Furthermore, other factors that influence arc deformation which are not modelled, for example back-arc spreading and changes in interplate stress unrelated to ridge subduction, must be considered separately from the effects of ridge subduction alone.

METHOD

The thin viscous sheet method developed by England & McKenzie (1982, 1983) for continental tectonics, is used for modelling the effects of ridge subduction. The thin viscous sheet models take into account vertical strain through the incompressibility condition and thus remove the restriction that the horizontal principal deviatoric stresses must be equal and opposite. Moreover, thin viscous sheet modelling takes into account stress arising from crustal thickness contrasts. For narrower zones of deformation that encompass island arcs, Geist & Scholl (1992) have applied this method to describe deformation of the Aleutian island arc resulting from changes in the obliquity of convergence. Rather than the elastic or viscoelastic theory used in previous models of ridge subduction, a power-law rheology based on experimental modelling of mantle and lower crustal rocks (Goetze 1978; Brace & Kohlstedt 1980) is used
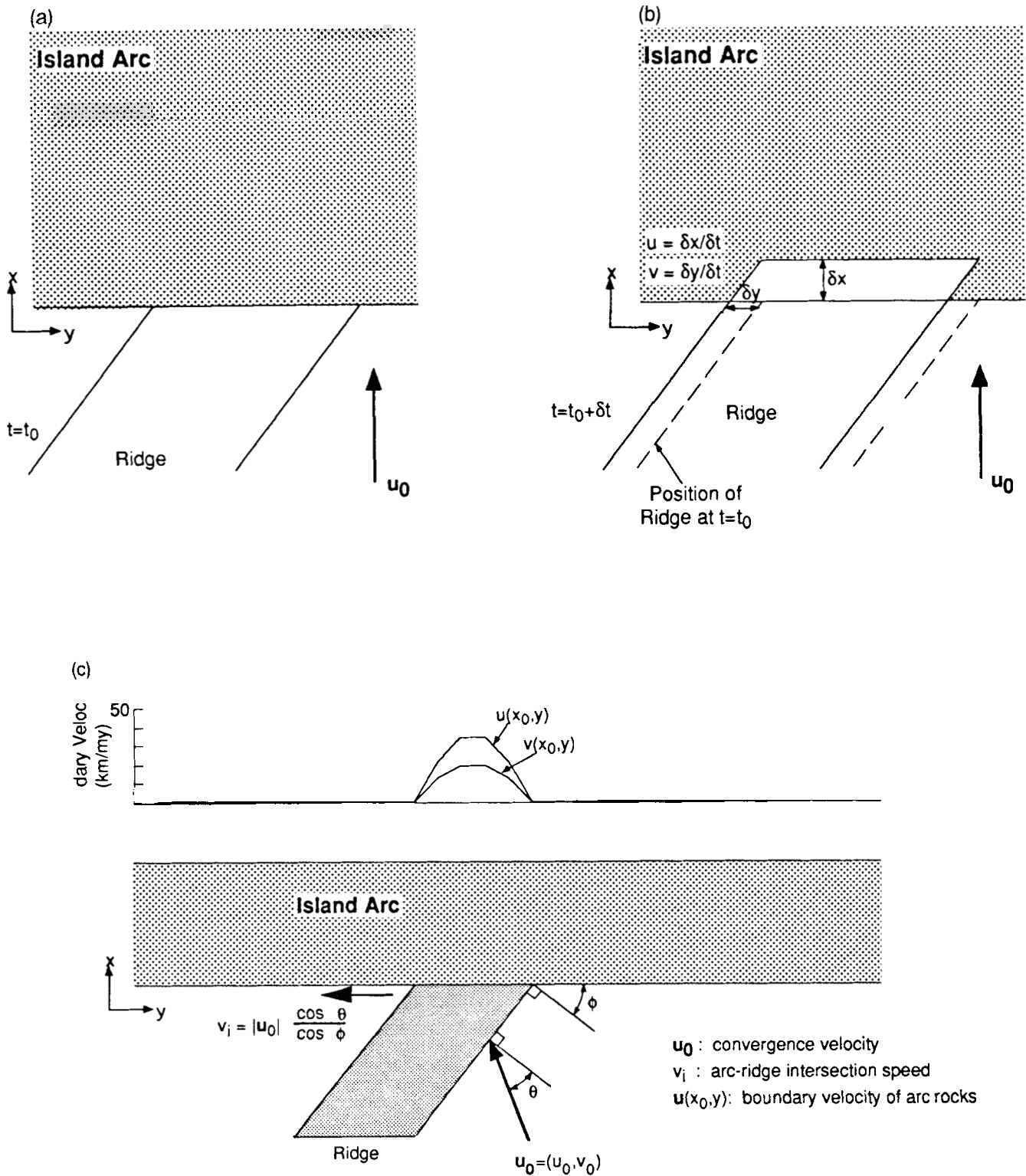
Figure 1. Diagram of velocity boundary conditions associated with ridge subduction. (a) and (b): explanation of 'snowplough' effect. (a) Ridge subduction normal to arc ($t = t_0$). (b) After a short amount of time (δt), island arc rocks at the boundary are moving parallel to the arc at a velocity proportional to the arc–ridge intersection speed (v_i) and normal to the arc at a velocity proportional to the normal component of the convergence velocity (u_0). (c) General case where orientation of ridge and convergence vector are arbitrary. Boundary velocity [taking into account the 'snowplough' effect as described in (a) and (b)] is separated into its arc-normal (u) and arc-parallel (v) components, whose positions at a particular time are dependent on the v_i, the speed of the arc–ridge intersection. A sinusoidal shape function is used to approximate a decrease in boundary velocity along the flanks of the ridge. See text for more explanation.
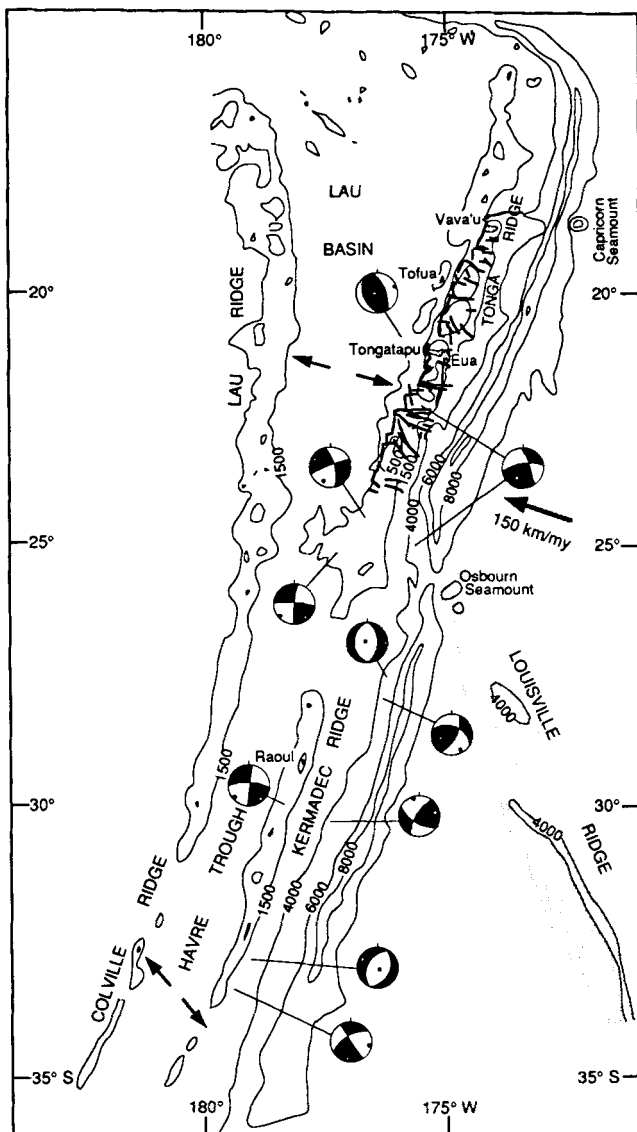
Figure 2. Bathymetry (in metres) and summary of arc deformation inferred to arise from ridge subduction along the Tonga arc. Heavy lines represent normal faulting within the arc massif (Dupont & Herzer 1985; Herzer & Exon 1985). Stippled area represents the Louisville Ridge. Focal mechanisms and the inferred direction of back-arc spreading (diverging arrows) from Pelletier & Louat (1989). Note that the arc is uplifted north of the arc–ridge intersection and downdropped south of the arc–ridge intersection.

in the development of the thin viscous sheet equation as described by England & McKenzie (1982). Because thin viscous sheet models consider deformation spanning millions of years, deformation is controlled by the strongest layer of the lithosphere, thought to be the upper mantle (Kirby 1980; Vilotte *et al.* 1982). For shorter term modelling, such as deformation associated with an earthquake cycle, elastic or viscoelastic models are more representative. The disadvantages of thin viscous sheet modelling are that analytical solutions are obtained for the simplest geometries only and that boundary conditions must be independent of depth. This limits the boundary conditions to horizontal shear and normal tractions and ignores the vertical

component of traction. For the two arcs, the dip of the subducting plate is steep, minimizing the downdip extent of the contact between the subducting plate and the arc, and thus minimizing the extent that the boundary conditions vary with depth. Also, with regard to boundary conditions, it should be noted that since the dip of the subducting plate beneath the New Hebrides arc is steeper than beneath the Tonga arc, the relative importance of vertical deformation at the collision zone may be different for the two arcs.

Assumptions

The assumptions used in thin viscous sheet modelling include those applicable for all continuum models and those specific to thin-sheet models. Continuum modelling assumes that no discontinuities exist within the deformation zone such that strain is distributed continuously. Thus, movement along a specific fault is not modelled, although the style of deformation can be derived from the strain-rate tensor (thrust, normal, or strike–slip). Thin viscous sheet models assume no shear traction at the base or top of the lithosphere (e.g. no asthenospheric corner flow). In addition, thin-sheet models in general require a large width to thickness ratio. For a linear rheology, the minimum ratio is approximately 3:1, as discussed by Artyushkov (1973) and Geist & Scholl (1992), which is approximately the dimensions of the Tonga and New Hebrides arcs. We use an arc lithosphere 80 km thick and 240 km wide for the models described here. Later in the paper, we verify that using the minimum thin-sheet dimensions does not introduce any spurious solutions. Two specific assumptions used in the development of the thin viscous sheet equation need to be examined in relation to modelling island arc deformation: (1) the effect of the vertical component of traction at the subduction zone boundary, and (2) stresses associated with small regions of uncompensated crustal thickening.

Effect of vertical shear traction at the subduction zone

Previous studies have shown that the topography near the trench is dynamically supported by the subducting slab (e.g. Sleep 1975; Forsyth 1980; Melosh & Raefsky 1980; Davies 1981; Tharp 1985; Zhang, Hager & Raefsky 1985; Sato & Matsu'ura 1988; Wdowinski 1992; Zhong & Gurnis 1992). Topography of the outer rise and trench is well matched by these models, however, it is unclear how far arcward the dynamic effects extend. It is also unclear whether the gravity anomaly across island arcs is caused by dynamic effects of the subducted slab (Davies 1981; Sato & Matsu'ura 1988; Zhong & Gurnis 1992) or by lateral variations in crustal density (modelled, for example, by Grow 1973; Collot & Malahoff 1982; Yang, Segaura & Fukuda 1992). The latter gravity models show that the density difference between the slab and the surrounding asthenosphere imparts a long-wavelength (>500 km) component to the total gravity anomaly. Using the crustal density structure for the New Hebrides arc determined by Collot & Malahoff (1982), topography is calculated assuming that the arc lithosphere is isostatically compensated and excluding the aforementioned dynamic effects at the trench and long-wavelength gravitational component (Fig. 4). In comparison to the actual topography, the isostatic topography is well matched
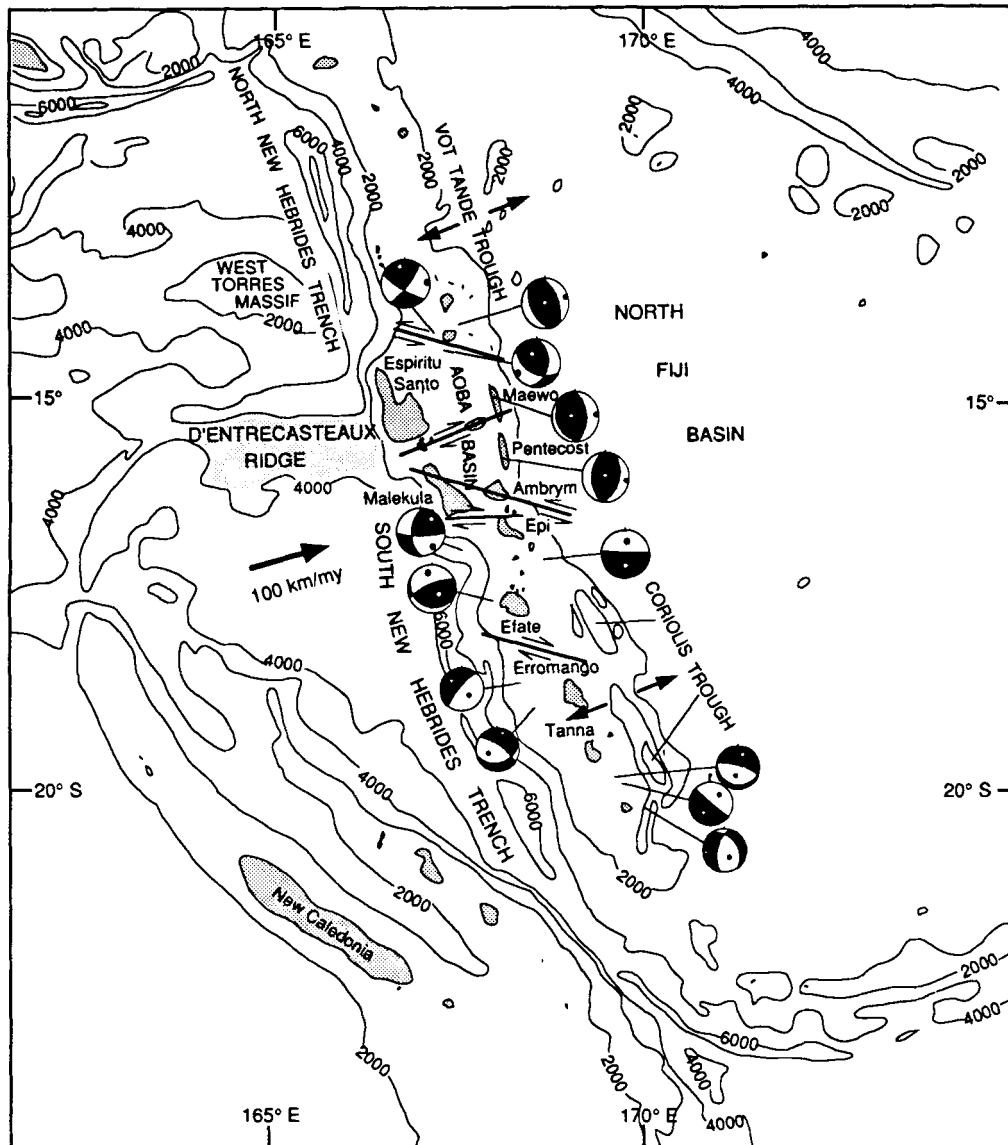
Figure 3. Bathymetry (in metres) and summary of arc deformation inferred to arise from ridge subduction along the New Hebrides arc. D'Entrecasteaux ridge and major islands stippled. Focal mechanisms from Isacks *et al.* (1981) and Louat & Pelletier (1989) and the inferred direction of back-arc spreading (diverging arrows) from Louat & Pelletier (1989). Transverse faulting mapped by Carney & Macfarlane (1982) and Greene *et al.* (1988).
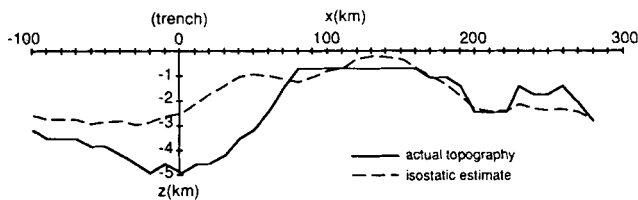

Figure 4. Comparison of the smoothed topography of the southern New Hebrides island arc to an isostatic estimate from gravity models. The isostatic estimate was calculated using the density structure given by Collot & Malahoff (1982) assuming Airy isostatic compensation and excluding dynamic effects and gravitational pull from the subducting slab.

at the arc massif and back-arc but deviates from the actual topography at the trench and forearc. This suggests that deviation from isostasy by dynamic support of island arc topography is significant within approximately 70 km of the trench.

Simple flexure models of the arc in response to a vertical end-load have been given by Walcott (1970), Chung & Kanamori (1978) and Turcotte & Schubert (1982). In the Appendix we estimate the vertical shear stress, assumed to be zero in thin viscous sheet theory, for the vertical end-load case. Numerical models of dynamic support by Davies (1981), Tharp (1985), Sato & Matsu'ura (1988) and Zhong & Gurnis (1992) more accurately predict island arc

topography than does the simple end-load flexure model. Although these models fit the general profile of outer rise, trench and back-arc topography, the anomalous elevation of the arc massif is underestimated by dynamic models. As discussed by Grow (1973), Sleep (1975) and Zhong & Gurnis (1992), elevation of the arc massif may be a result of low-density crust localized along the ridge axis.

From the gravity-derived estimate of isostasy and from the simple flexure and numerical models described above, significant dynamic uplift of island arc topography is dominant within approximately 50–70 km arcward of the trench (Figs 4 and A1). Farther from the trench, the arc is dominated by horizontal compressive stress, as indicated by numerical and physical models (Tharp 1985; Shemenda 1992). The horizontal stresses are modelled by thin viscous sheet theory as they relate to horizontal shear and normal traction at the subduction zone. Crustal thickening predicted by the thin viscous sheet models is generated by horizontal compression; deformation caused by the vertical component of traction at the subduction zone is not modelled and is likely to be important within 50–70 km of the trench.

Effect of local regions of uncompensated crust

Local regions of crustal thickening smaller than 100 km develop during the thin viscous sheet modelling of ridge subduction and may not be completely compensated at depth. In the derivation of the thin viscous sheet equation, the condition of isostasy implies that pressure at the base of the lithosphere (below the depth of compensation) is constant and that the topography is dependent only on the crustal thickness and the average crust and mantle densities. To determine the inaccuracy in the model caused by stresses associated with a completely uncompensated feature (i.e. no crustal root), we apply the analysis by Fleitout & Froidevaux (1982) to estimate these stresses as a function of wavelength. The resulting estimate of stress is considered a maximum because the feature will probably be increasingly compensated with increasing wavelength.

Fleitout & Froidevaux (1982) derive expressions for the stresses associated with a mass heterogeneity at the Moho as a function of wavelength of the heterogeneity. For the case of a completely uncompensated crustal feature, the mass heterogeneity is the difference between mantle and crustal densities for the volume of the missing crustal root. The horizontal and vertical normal stresses at the surface as a function of wavenumber are shown in Fig. 5. The curves in Fig. 5 were calculated for a model consisting of a linearly viscous crust overlying an inviscid mantle (Fleitout & Froidevaux 1982). For a large feature (as wavenumber→0), the vertical normal stress equals the weight of excess mass at depth (such a feature should be completely compensated). For smaller features, the vertical and horizontal normal stresses approach zero. The average wavelength of crustal thickening from our ridge subduction models is approximately 50 km, which, if completely uncompensated, results in approximate magnitudes of 5 MPa and 10 MPa for the horizontal and vertical stress, respectively. Thus, although regions of uncompensated crustal thickening may affect deformation locally, the associated stress magnitudes are substantially below the stress magnitudes associated with ridge subduction.
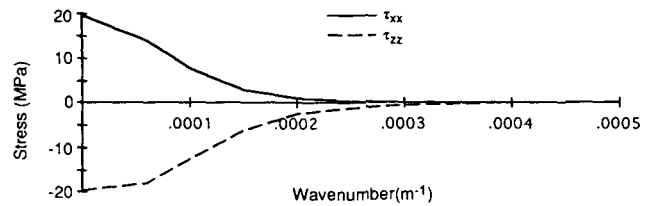

Figure 5. Estimate of surface stress associated with uncompensated regions of crustal thickening. Horizontal (solid line) and vertical (dashed line) normal stresses are plotted against the wavenumber (inverse of wavelength) of the feature. Curves calculated from equations derived by Fleitout & Froidevaux (1982). As the wavelength of the uncompensated feature decreases (wavenumber increases), the associated surface stresses exponentially decrease. See text for more explanation.

Physical parameters

The physical properties that are independent variables in the model are the power-law exponenent n and the Argand number Ar defined by England & McKenzie (1982) as

$$Ar = \frac{g\rho_c(1 - \rho_c/\rho_m)L^{(1 + 1/n)}}{Bu_0^{1/n}}, \quad (1)$$

where g is the gravitational acceleration, L is the thickness of the lithosphere, u_0 is the characteristic convergence velocity, ρ_c and ρ_m are the crust and mantle densities, respectively, and B is a constant in the power-law relation that includes the temperature dependence of vertically averaged rheology. The Argand number is inversely related to the ability of the lithosphere to sustain crustal thickness contrasts, or equivalently, inversely related to the vertically integrated strength of the lithosphere as explained by Sonder & England (1986). With respect to the effective power-law exponent n, low values result in diffuse deformation, while higher values of n result in shear thinning, a property whereby deformation is concentrated in the regions of highest stress (England & McKenzie 1982). The value for n ranges between 2 and 5 for most crustal and mantle rocks (Brace & Kohlstedt 1980; Kirby 1983; Kirby & Kronenberg 1987). The vertically averaged rheology can also be approximated by power-law flow as shown by Sonder & England (1986). Higher values of n have been used to include an increasing dominance of brittle deformation in the lithospheric average of n (Sonder & England 1986), but such values are not used for models described in this study because of instability for n greater than 5.

Boundary conditions

The same dimensions for the arc and ridge were used for each set of models. The width of the arc is 240 km; the width of the converging oceanic ridge is 100 km; the thickness of the lithosphere is 80 km; and the initial thickness of the arc crust is 17 km. The latter value is approximately the average crustal thickness deduced from seismic refraction studies of the New Hebrides and Tonga arcs (Pontoise & Latham 1982; Pontoise, Latham & Ibrahim 1982). The width of the arc remains fixed for the duration of the model, implying that new crustal material is added to

the arc to compensate for horizontal shortening. The boundary conditions and direction of arc–ridge propagation are different for the two cases.

To analyse the effect of arc–ridge intersection speed on deformation, two arcs with similar characteristics are considered: Tonga and New Hebrides. For these arcs, the rate of convergence and duration of ridge subduction (up to the present time) is approximately the same. Likewise, the Louisville and d'Entrecasteaux ridges have approximately the same width. This leaves the intersection speed and physical properties of the arcs as the primary independent variables.

Velocity boundary conditions that vary with time corresponding to the propagation of the ridge–arc intersection are specified on the active (frontal) side of the arc. At first, it might seem that the orientation of the boundary velocity of arc rocks would be parallel to the convergence vector, which is independent of the arc–ridge intersection speed (v_i). However, what we are really interested in is the speed and direction of arc rocks being deformed by the subducting ridge (termed the 'snowplough' effect by Bouysse & Westercamp 1990). Consider a situation where the convergence vector is normal to the arc (Fig. 1a). Then suppose that after a small amount of time (δt), the ridge indents the arc before being subducted (Fig. 1b). The speed of arc rocks parallel to the trend of the arc is proportional to the arc–ridge intersection speed ($\delta y/\delta t$); the speed of arc rocks normal to the arc is proportional to the normal component of the convergence vector ($\delta x/\delta t$). For convergence subnormal to the arc, v_i also depends on the tangential component of the convergence velocity, as described below. The boundary velocity of arc rocks outside the arc–ridge collision zone is zero, such that only deformation associated with ridge subduction is modelled. Inside the collision zone, the velocity is given by the following equations (Fig. 1c):

$$u(x_0, y) = \alpha u_0 \sin\left[\frac{\pi}{(w_r/\cos\phi)}(y + y_0 \pm v_i t)\right] \qquad (2)$$

and

$$v(x_0, y) = \alpha v_i \sin\left[\frac{\pi}{(w_r/\cos\phi)}(y + y_0 \pm v_i t)\right], \qquad (3)$$

where w_r is the width of the ridge; y_0 is the initial position of the arc–ridge intersection; v_i is the speed of the arc–ridge intersection; u and v are the x and y components of the velocity vector, respectively [i.e. $\mathbf{u} = (u, v, w)$]; u_0, v_0, are the x and y components, respectively, of the convergence velocity vector; and α is a proportionality constant that represents the fraction of converging plate velocity transferred to the overriding plate. The choice of the plus or minus sign in eqs (2) and (3) determines the direction of arc–ridge propagation. A sinusoidal rather than a square-shape function is used to best represent a decrease in boundary velocity along the flanks of the ridge. The peak velocity within the collision zone must be a fraction of the converging plate velocity to allow for subduction (i.e. $\alpha < 1$). That is, the subducting ridge must be moving faster than the arc rocks at the boundary. For α less than about 0.5, the magnitude of stresses is linearly dependent on α while the orientation of stress does not vary. A value of $\alpha = 0.2$ is used for all of the models.

The speed of the arc–ridge intersection (v_i) depends on the speed of convergence and the orientation of the convergence vector, ridge, and arc. For θ and ϕ shown in Fig. 1(c), v_i is given by the following equation:

$$v_i = |\mathbf{u}_0| \frac{\cos\theta}{\cos\phi}, \qquad (4)$$

where $|\mathbf{u}_0|$ is the speed of convergence:

$$|\mathbf{u}_0| = (u_0^2 + v_0^2)^{1/2}. \qquad (6)$$

Alternatively, the boundary conditions can be stated in terms of stress, as discussed by Sonder, England & Houseman (1986) and Wdowinski & O'Connell (1990). However, for the New Hebrides and Tonga arcs more is known about the boundary velocities than the boundary stresses. Evidence for increased boundary stress, and therefore increased boundary velocity, where ridges are subducted results from observations of interplate and shallow earthquakes (Isacks *et al.* 1981; Marthelot *et al.* 1985; Christensen & Lay 1988; Louat, Hamburger & Monzier 1988; Chantelain & Grasso 1992).

Using these boundary conditions, the thin viscous sheet equation is solved using its finite difference approximation and a cyclic reduction algoithm as described by England & McKenzie (1982). Crustal thickness and the position of the arc–ridge intersection are updated for each time step. The time step is chosen for stability and differs for each set of parameters tested.

FAST ARC–RIDGE PROPAGATION: TONGA–LOUISVILLE

The methodology used to analyse ridge subduction is to first determine how arc deformation responds to different values of n and Ar and then to evaluate the different models with respect to structures formed during ridge subduction. Focal mechanisms from intra-arc earthquakes are also compared to the model results with the recognition that these earthquakes relate to the entire subduction process that includes ridge subduction. Values for the rate of convergence at the Tonga trench reported by Dupont & Herzer (1985), using the RM-2 model of Minster & Jordan (1978) and by taking into account Lau Basin spreading, range between 120 and 150 km Myr^{-1} at the latitude of the Louisville ridge (Lonsdale 1986; Ballance *et al.* 1989; Pelletier & Louat 1989). This results in a range of 140–180 km Myr^{-1} for the southward propagation of arc–ridge intersection. An intersection speed of 180 km Myr^{-1} is used for this study. The duration of ridge subduction is estimated by Dupont & Herzer (1985) to be 3.0–3.5 Myr, during which time the arc–ridge intersection progressed approximately 550–600 km along the trench. Solutions for the principal stresses, style of faulting, crustal thickening and finite rotation are used to analyse the models.

Model results

We first describe the characteristics for $n = 1$ and $Ar = 0$ (lithosphere characterized by high vertically integrated strength and diffuse deformation) and use this as a foundation to describe the changes in deformation by

varying *n* and *Ar*. The principal stresses shown in Fig. 6(a) are greatest at the collision zone and diminish exponentially in magnitude away from the collision zone. Leading the collision zone (southward), the orientation of principal compressive stress radiates away from the collision zone, whereas in the wake of the collision zone (northward), the principal tensional stress is oriented primarily subparallel to the arc. The mnemonics shown in Fig. 6(a) describe the style of faulting and are derived from the strain-rate tensor (Houseman & England 1986; Bird 1989). The first letter denotes the primary style while the second letter denotes for the secondary style of either thrust (T), normal (N), or strike–slip (S). For example, SN describes a region of major strike–slip faulting with a minor normal component; TT describes a region where thrust faulting is parallel to both principal stress axes. For the model shown in Fig. 6(a), the largest stress magnitudes are associated with strike–slip faulting with a minor thrust component ahead of the collision and a region dominated by normal faulting (NN–NS) 50–100 km in the wake of the collision zone.

Crustal thickening, due to ridge subduction, for this model (Fig. 6b) reaches a maximum at the collision zone and forms a plateau extending across the arc in the wake of the collision. Thus, crustal thickening that arises from ridge subduction is preserved after the passage of the ridge. Away from the collision zone, crustal thickening is slightly greater at the frontal part of arc than at the back. The absolute amount of crustal thickening depends directly on the proportionality constant α. The seemingly contradictory occurrence of thickened crust and transverse normal faulting can be explained by the fact that the thickened crust is a result of accumulated shortening strain while transverse normal faulting is a manifestation of instantaneous strain (England 1982). It is interesting to note that the arc-parallel asymmetry in the crustal thickening map caused by the propagation of the arc–ridge intersection is similar to the asymmetry in uplift found for subduction of the Nazca ridge beneath South America (Macharé & Ortlieb 1992).

The greatest amount of finite rotation about a vertical axis occurs directly ahead of the collision zone (Fig. 6c). Finite rotation was calculated by integrating half of the vertical component of vorticity over the duration of the model, and describes small rigid-body rotation as opposed to rotation of material vectors (McKenzie & Jackson 1983). Rotation ahead of the collision zone is positive (counter-clockwise) while a smaller amount of negative values (clockwise rotation) occurs behind the collision zone. As the ridge progresses southward along the arc, the region of negative rotation following the ridge negates the region of positive rotation that formed ahead of the ridge at an earlier time, resulting in no net vertical axis rotation. The region of negative rotation in the northern part of the model is an artefact stemming from the initiation stage of the model that was not negated by an earlier positive rotation. As with the values for crustal thickness, the absolute magnitude of rotation depends directly on α.

We now calculate how deformation changes by increasing the stress–strain exponent *n* (increasing the effect of shear thinning). As *n* increases, the zone of dominant arc-parallel tensional stress in the wake of the collision zone disappears and a radiating compressive stress field both leading and following the point of arc–ridge intersection becomes more

apparent (Fig. 7a). Consequently, the faulting style throughout the arc involves either a major or minor component of thrusting. Also, the magnitude of stress away from the collision zone increases with increasing *n*. As a consequence of shear thinning, the greatest crustal thickening occurs closer to the frontal edge of the arc with increasing *n*, without a plateau developing as with the $n = 1$ case (Fig. 7b). The fact that the maximum in crustal thickening is preserved with the passage of the ridge can be explained by the reduced effect of tensional stress that acts to reduce the crustal thickness within 50–100 km of the collision zone for the $n = 1$ case. Thus, increasing *n* causes more localized but also more intense uplift. Similarly, the high amount of counter-clockwise rotation ahead of the collision zone for $n = 1$ disappears and a constant amount of clockwise rotation is preserved with the passage of the ridge for increasing *n* (Fig. 7c). The latter is explained by the lack of counter-clockwise rotation ahead of the ridge needed to negate the effects of clockwise rotation following the ridge, as with the $n = 1$ case.

The value of *Ar* regulates the importance of buoyancy stresses derived from gradients in crustal thickness. Because the models of ridge subduction span only a few million years and do not generate large crustal thickness variations, the results of the models are somewhat insensitive to *Ar*. Increasing *Ar* to high values (descreasing the vertically integrated strength of the lithosphere), increases the magnitude of stress along the edges of the arc away from the collision zone (Fig. 8). The magnitude of the two principal horizontal stresses are similar here, indicating relatively high shear stress along the edges of the model. The zone of normal faulting in the wake of the collision zone persists with higher *Ar*, although it becomes more restricted in lateral extent. As *Ar* increases to very high values (> 1000), deformation tends to be limited to plane horizontal strain as explained by Sonder & England (1986) and horizontal flow takes precedence over vertical thickening or thinning of the crust.

Observations

The general structural characteristics associated with ridge subduction along the Tonga arc are uplift of the entire massif and pervasive normal faulting of the arc crest transverse to the trend of the arc north of the Louisville ridge intersection point. As shown in Fig. 2, the area enclosed by the 1500 m contour is significantly greater north of the arc–ridge intersection than it is south of the intersection. Directly south of the collision zone, the bathymetry of the arc crest slopes downward approximately 2 km before rising to the crest of the Kermadec arc. In addition, a recent seabeam survey of the region indicates horizontal shortening and uplift at the latitude of the present arc–ridge intersection (Pelletier & Dupont 1990; Lallemand *et al.* 1992). From this evidence we assume that crustal thickening of the arc from the latitude of the Louisville ridge to the north is related to ridge collision and not effects from back-arc spreading or differences in the rate of constructional magmatism at the latitude of the Louisville ridge.

Structural and stratigraphic interpretation of seismic reflection data, along with studies of emerged coral-reef terraces indicate uplift, transverse normal faulting and block
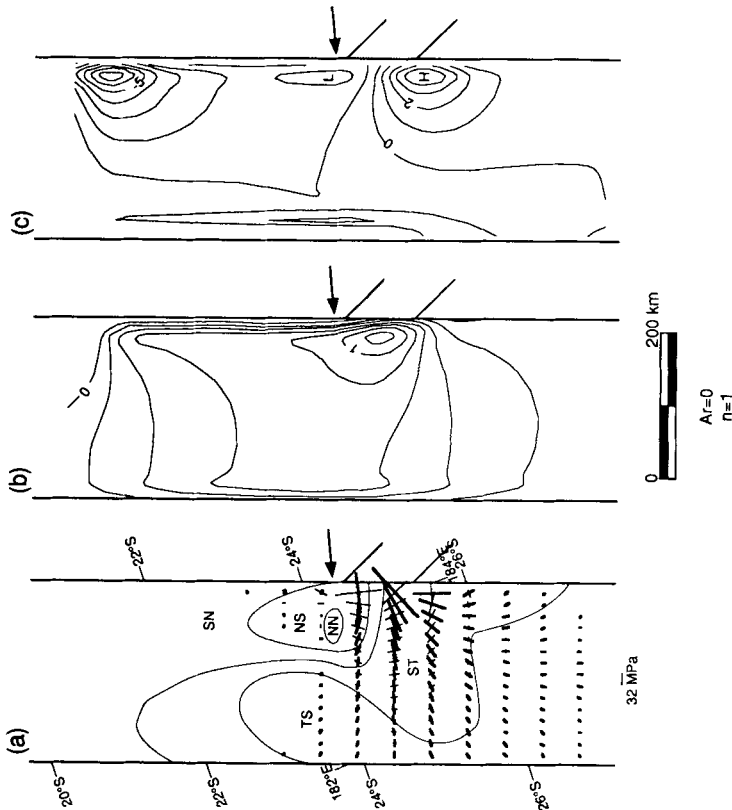
Figure 7. Effect on deformation by varying n ($n = 1, 3$ and 5) and holding Ar constant ($Ar = 0$) for Tonga-type ridge subduction. Increasing n increases the overall magnitude of stress and localizes the permanent deformation near the frontal part of the arc. (a) Principal horizontal stresses and style of faulting after 3 Myr. Heavier line indicates compressive stress. (b) Crustal thickening due to ridge subduction in kilometres. Contour interval is 0.2 km for each plot. (c) Amount of vertical finite rotation for small elements measured in degrees (positive is counter-clockwise). Contour interval is 1° for each plot.

Figure 6. Deformation resulting from $Ar = 0$ and $n = 1$ after 3 Myr for Tonga-type ridge subduction. (a) Principal horizontal stresses with heavier line indicating compressive stress. Regions with a similar style of faulting separated by thin continuous line and are denoted by a two-letter mnemonic corresponding to the two possible styles of deformation. (T, thrust; N, normal; S, strike–slip) (b) Crustal thickening due to ridge subduction in kilometres assuming an initial thickness of 17 km. Contour interval is 0.2 km. As discussed in the text, the topography of the ridge is dominated by dynamic effects from subduction within approximately 70 km of the trench. (c) Amount of vertical finite rotation for small elements measured in degrees (positive is counter-clockwise). Contour interval is 1°. Amount of crustal thickening and finite rotation are dependent on values chosen for α.
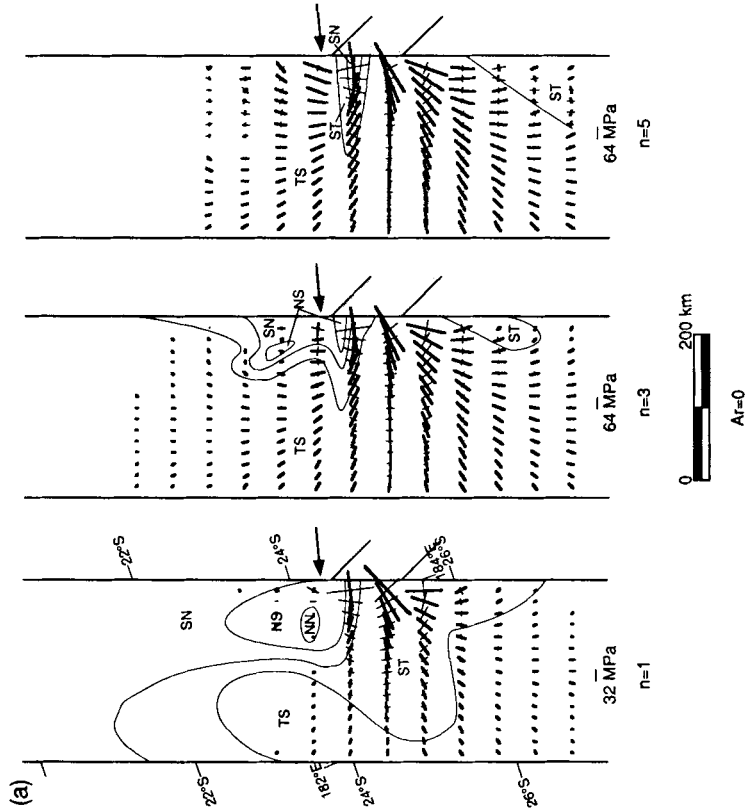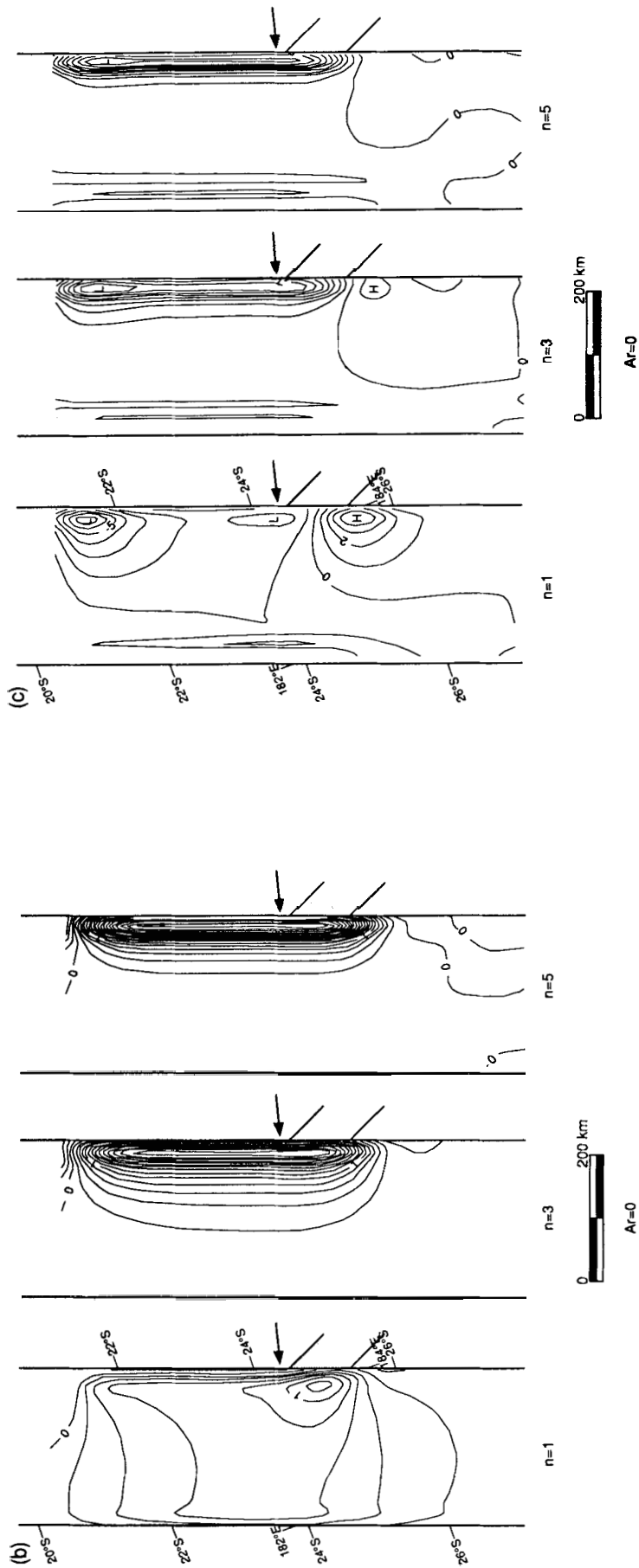
Figure 7. (*Continued.*)

tilting of the Tonga arc massif, north of the latitude of the Louisville ridge. Transverse normal faulting in the wake of ridge subduction has been mapped using seismic reflection data between 21° and 23°S by Herzer & Exon (1985) and extrapolated northward as far as 18°S and southward to the collision zone, based on bathymetry by Dupont & Herzer (1985) (Fig. 2). These faults, in most cases, bound structural domes, further indicating uplift of the arc massif in the wake of ridge subduction (Dupont & Herzer 1985). Seismic stratigraphic studies indicate a north-to-south migration of depocentres, with a similar migration of sediment provenance (Austin, Taylor & Cagle 1989). Furthermore, by dating and measuring the altitude of emerged coral reefs, Taylor (1978) concludes that the southernmost structural block (including the islands of Eua and Tongatapu, Fig. 2) have emerged in Holocene time, while the northernmost blocks (including the island of Vava'u) have subsided. All of these authors ascribe the progressive north-to-south uplift and arc-parallel tensional structures to subduction of the Louisville ridge.

Intra-arc earthquakes for which focal mechanism solutions are available is sparse north of the collision zone and slightly more abundant south of the collision zone (Fig. 2). Pelletier & Louat (1989) find 79 focal plane solutions from 1964 to 1987 after eliminating the interplate thrust solutions. However, most of these earthquakes are not related to ridge subduction and include normal and strike–slip earthquakes in the Lau–Havre Basin region or earthquakes located either at the northern terminus of the Tonga arc or within the Pacific plate. Just north of the collision zone there are two strike–slip solutions with a small thrust component (ST). Two different sets of focal mechanism have been determined south of the collision zone: strike–slip with minor thrusting (ST) and almost pure normal faulting (NS–NN).

Lacking a consistent picture of deformation from the focal mechanisms, we evaluate the previous models largely on the basis of structural data. Normal faulting, structural doming and crustal thickening in the wake of ridge subduction corresponds closely with low values of both Ar and n. Because the area of highest tensional stresses predicted by this model precedes the passage of the ridge by 50–100 km, displacement rates on normal faults should progressively diminish farther to the north. There is some indication of high-angle faulting of the ridge crest ahead of the Louisville ridge from Soviet single channel data (Anosov *et al.* 1983; Gnibidenko *et al.* 1985), although it is insufficient to confirm whether or not compressional deformation is present here as predicted by the models. The high amount of counter-clockwise rotation shown in the models leading the ridge may explain the indentation and complex bathymetry of the trench slope directly south of the ridge intersection.

SLOW ARC–RIDGE PROPAGATION: NEW HEBRIDES–D'ENTRECASTEAUX

The same methodology that was used in the previous section is used to analyse subduction of the d'Entrecasteaux ridge. The speed for the New Hebrides–d'Entrecasteaux intersection is almost an order of magnitude less than for the Tonga–Louisville system, even though the convergence rates are comparable. Greene *et al.* (1988), Louat &

Pelletier (1989) and Collot & Fisher (1991) estimate 90–100 km Myr^{-1} for the rate of convergence using the RM-2 model (Minster & Jordan 1978). This results in a northward propagation rate of approximately 25 km Myr^{-1} for the arc–ridge intersection. The duration of subduction is approximately 3–4 Myr (Greene *et al.* 1988). As before, we use solutions for the principal stresses, style of faulting, crustal thickening and finite rotation in order to analyse the models.

Model results

For the model where $Ar = 0$ and $n = 1$, the stress field rapidly diminishes in magnitude and radiates away from the collision zone and a region of thrust faulting with subordinate strike–slip faulting (TS) dominates the region directly arcward of the collision zone (Fig. 9a). There are also zones of high tensional stress adjacent to the collision corresponding to the SN and NS regions of faulting. Responding to these stresses, crustal thickening is greatest just arcward from the point of collision, with a small ridge of thickened crust developing along the back edge of the arc (Fig. 9b). Crustal thinning occurs in the wake of ridge propagation along the frontal edge of the arc. A bipolar pattern of finite rotation is associated with the slow propagation model, with clockwise rotation south of the ridge and counter-clockwise rotation north of the ridge (Fig. 9c). The magnitude of the rotation is greatest in the wake of ridge propagation. The asymmetry in the stress, crustal thickening and finite rotation fields indicates that even a slow intersection speed has a significant effect on deformation.

As n increases, changes in the stress field and faulting regime are most apparent away from the collision zone, whereas compressional stress and thrust faulting dominate the region directly arcward of the collision zone (Fig. 10a) for all values of n tested. At the collision zone, the magnitude of stress is greater with increasing n and does not diminish away from the collision zone as rapidly. Regions of normal/strike–slip faulting (SN–NS) adjacent to the central zone of the thrust/strike–slip faulting (ST–TS) also persists for all values of n. As n increases, both the small region of thickening near the back of the arc and the region of crustal thinning following the propagating ridge (southward) disappear (Fig. 10b). As a result of shear thinning with increasing n, the amount of crustal thickening directly in front of the collision zone (northward) increases and becomes more compressed against the front of the arc. Also, the bipolar nature of the rotation field is destroyed leaving only a region of high amounts of clockwise rotation in the wake of the subducting ridge (Fig. 10c).

The result of increasing Ar for the New Hebrides arc is similar to that for the Tonga arc. As Ar increases, shear stress increases along the edges of the arc (Fig. 11) reflecting the increased dominance of horizontal flow.

Two-ridge boundary condition

We now investigate how varying the morphology of the subducting ridge affects the large-scale deformation. The fact that the d'Entrecasteaux ridge is actually composed of two parallel ridges has been shown to have an important influence on deformation at the arc margin (Collot *et al.*
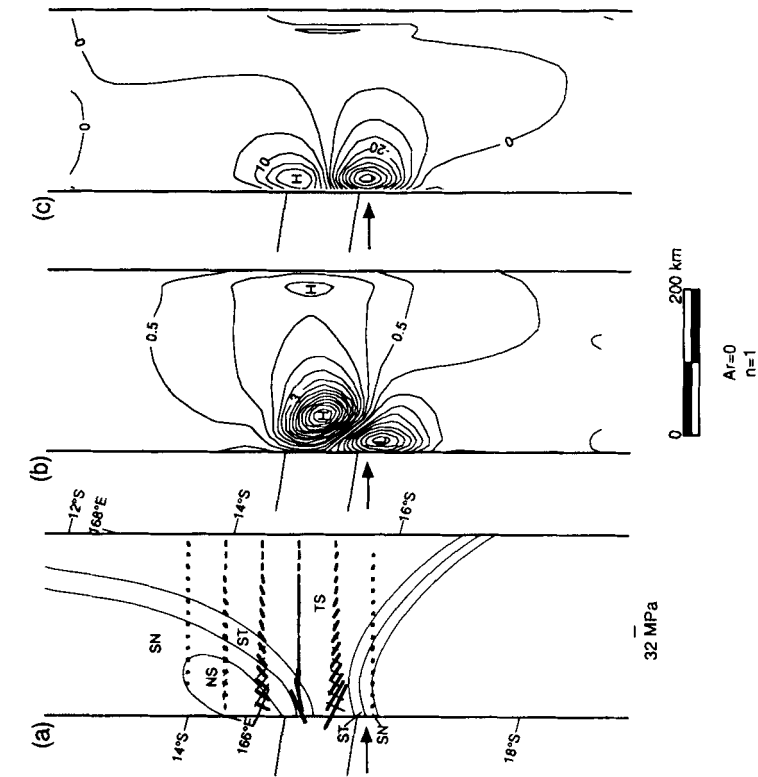
Figure 9. Deformation resulting from $Ar = 0$ and $n = 1$ after 3 Myr for New Hebrides-type ridge subduction. (a) Principal horizontal stresses and style of faulting. Heavier line indicates compressive stress. (b) Crustal thickening due to ridge subduction in kilometres. Contour interval is 0.5 km. (c) Amount of vertical finite rotation for small elements measured in degrees (positive is counter-clockwise). Contour interval is 5°. Amounts of crustal thickening and finite rotation are dependent on values chosen for α.
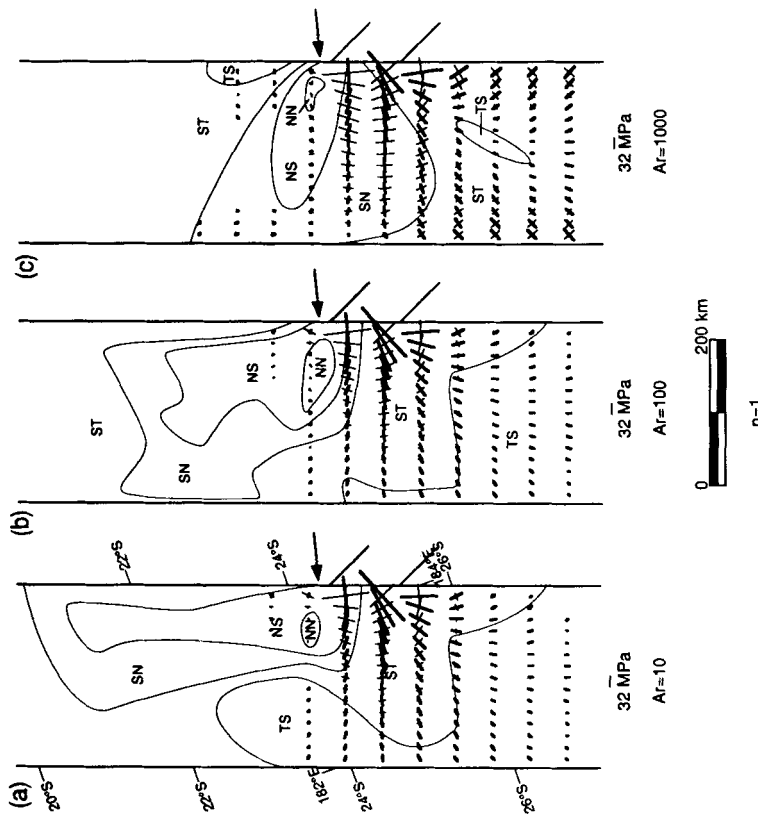
Figure 8. Effect on principal horizontal stresses and style of faulting after 3 Myr by varying Ar and holding n constant ($n = 1$) for Tonga-type ridge subduction. Heavier line indicates compressive stress. Increasing Ar increases the magnitude of shear stress near the edges of the arc (denoted by similar magnitudes of principal stresses) and decreases the crustal thickness contrasts. (a) $Ar = 10$, (b) $Ar = 100$ and (c) $Ar = 1000$.
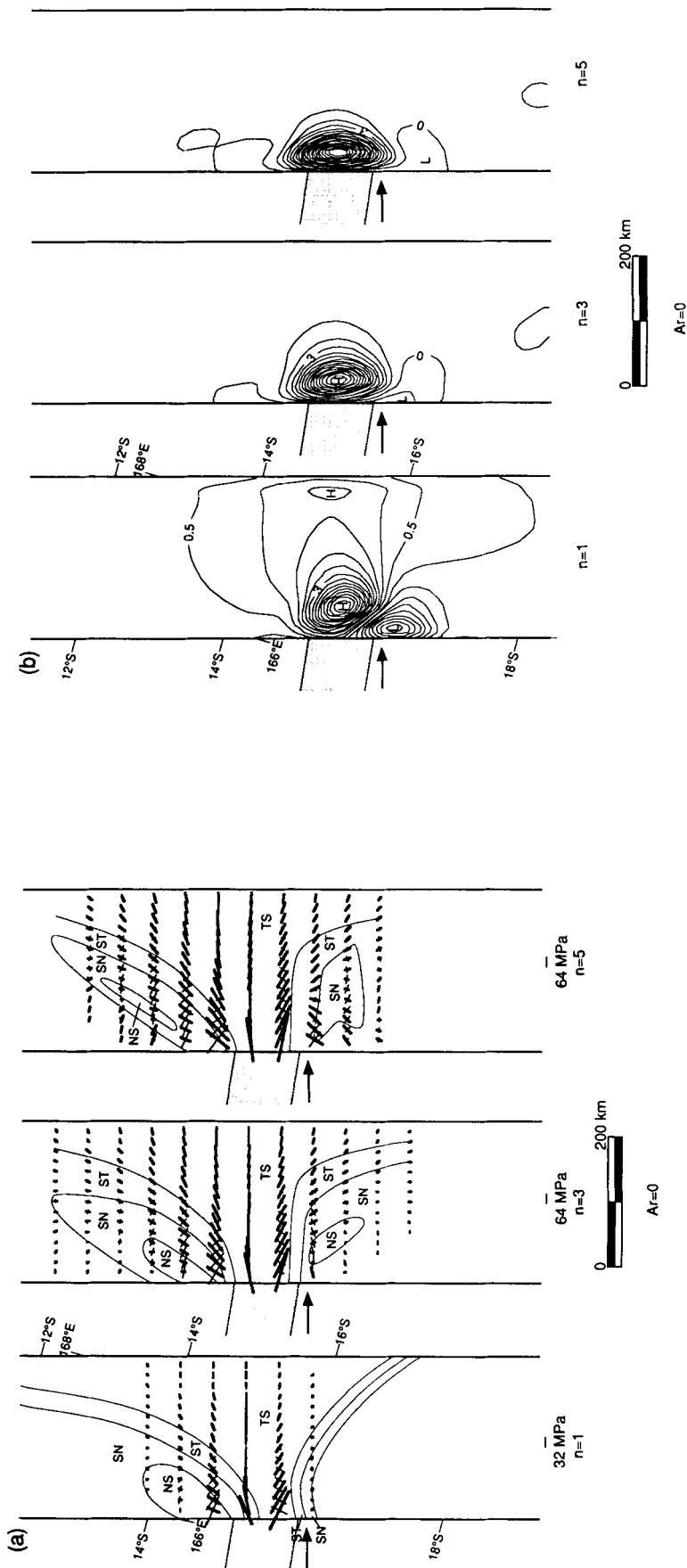
Figure 10. Effect on deformation by varying n ($n = 1$, 3 and 5) and holding Ar constant ($Ar = 0$) for New Hebrides-type ridge subduction. Increasing n increases the overall magnitude of stress and localizes the permanent deformation near the frontal part of the arc. (a) Principal horizontal stresses and style of faulting after 3 Myr. Heavier line indicates compressive stress. (b) Crustal thickening due to ridge subduction in kilometres. Contour interval is 0.5 km for $n = 1$ and 1.0 km for $n = 3$ and 5. (c) Amount of vertical finite rotation for small elements measured in degrees (positive is counter-clockwise). Contour interval is 5° for $n = 1$ and 3 and 10° for $n = 5$.
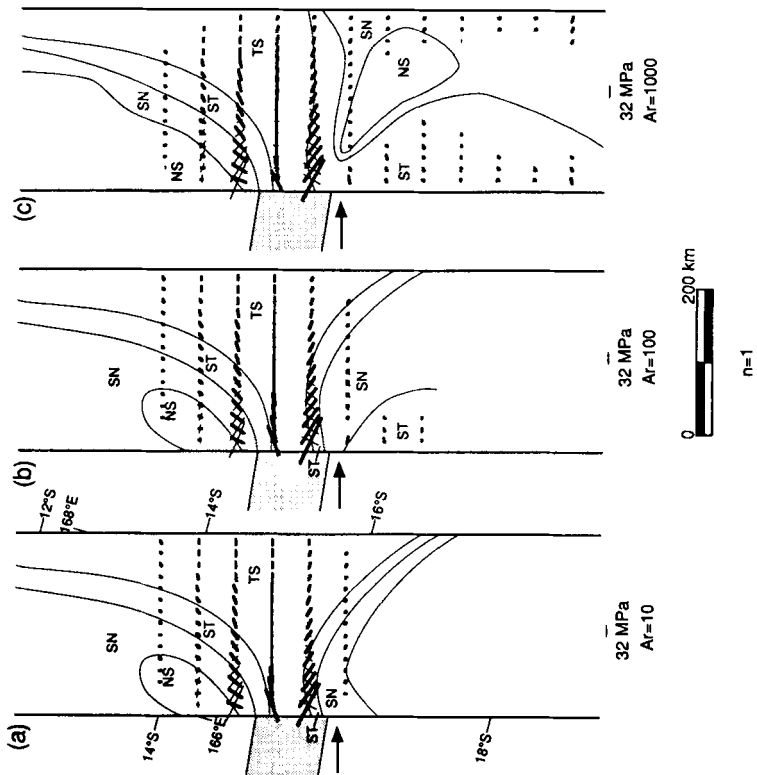
Figure 11. Effect on principal horizontal stresses and style of faulting after 3 Myr by varying Ar and holding n constant ($n = 1$) for New Hebrides-type ridge subduction. Heavier line indicates compressive stress. Increasing Ar increases the magnitude of shear stress near the edges of the arc (denoted by similar magnitudes of principal stresses) and decreases the crustal thickness contrasts. (a) $Ar = 10$, (b) $Ar = 100$ and (c) $Ar = 1000$.
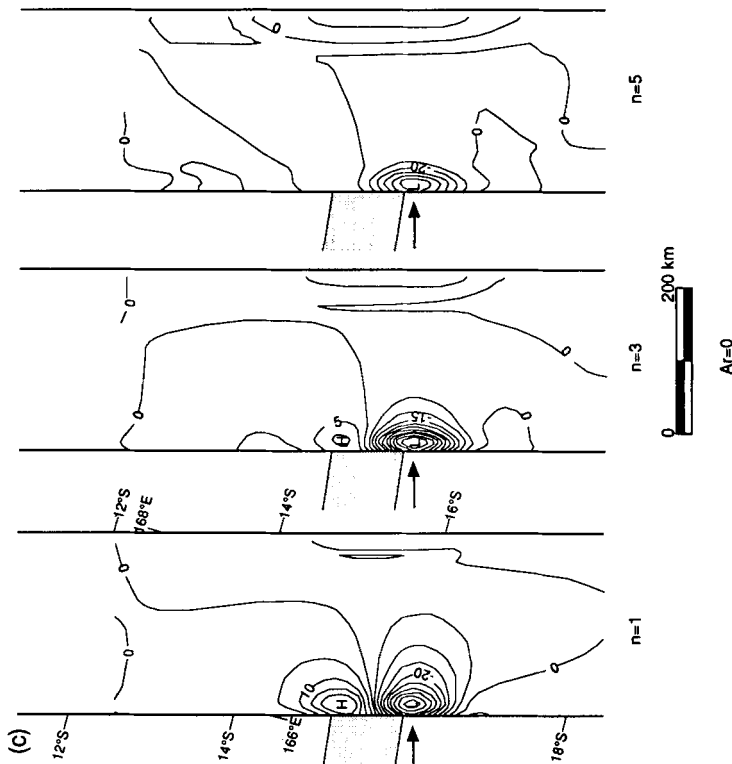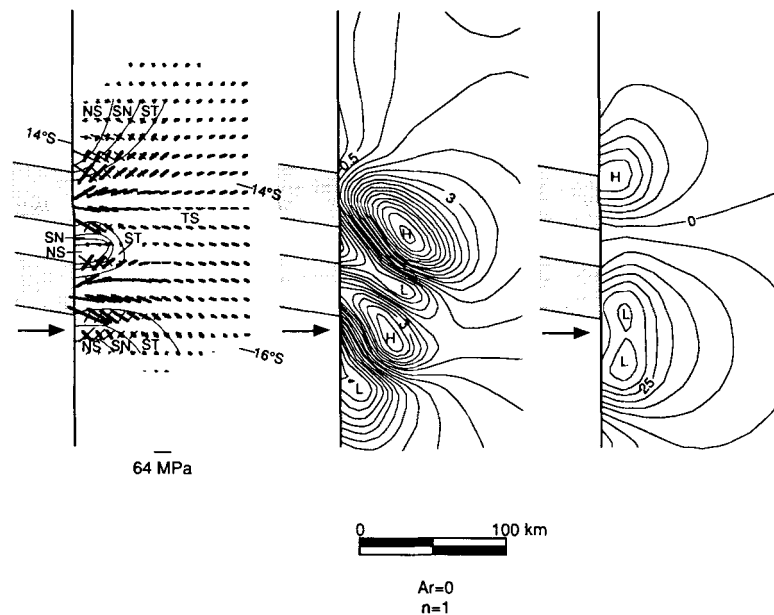
Figure 10. (*Continued.*)

Figure 12. Effect of using two parallel ridges as a boundary condition rather than a single ridge. Only the region near the collision zone is shown. (a) Principal horizontal stresses and style of faulting. Heavier line indicates compressive stress. (b) Crustal thickening due to ridge subduction in kilometres. Contour interval is 0.5 km. (c) Amount of vertical finite rotation for small elements measured in degrees (positive is counter-clockwise). Contour interval is 5°. Amount of crustal thickening and finite rotation are dependent on values chosen for α.

1985; Fisher 1986; Fisher *et al.* 1986, 1991; Collot & Fisher 1991). Although the models presented in this study do not have the resolution to predict the detail of structures described by these authors, we test the two-ridge boundary condition to observe its effect on large-scale deformation (Fig. 12). The stress field within approximately 50 km of the collision zone is complicated, but can be characterized by a radiating trend of principal compressive stress about each ridge (Fig. 12a). Farther away from the collision zone, the stress field is similar to that for a single subducting ridge. The region of thickened crust adjacent to the collision is separated into two lobes using the two-ridge boundary condition (Fig. 12b). Although it is difficult to evaluate whether an elongated region of thinner crust separating these two lobes exists, such a region does correspond in location to the channel separating the islands of Espiritu Santo and Malekula (Fig. 3). The two-ridge boundary condition also creates a slightly larger region of clockwise vertical axis rotation than the single-ridge boundary condition (Fig. 12c).

Test of applicability of thin sheet dimensions to island arcs

Thin viscous sheet models assume that the width of the deformation zone is much greater than its thickness, such that the vertical variation of horizontal velocity and hence vertical shear stress is insignificant. These conditions are fulfilled if $x_w/L > 3$ (where x_w is the width of the arc) for a Newtonian fluid (Artyushkov 1973). Geist & Scholl (1992) estimated the error associated with narrow deformation zones as a function of the width of the arc. They showed that the error abruptly increases for $x_w/L < 3$ and gradually increases for fixed x_w as n increases. In order to model island arc deformation between an active boundary (subduction zone) and a passive or 'rigid' boundary, we are

required to keep the minimum width-to-thickness ratio. Fig. 13 shows the results of an additional test of the thin sheet assumption applied to island arc deformation. Fig. 13(a) shows the New Hebrides crustal-thickening map for $Ar = 0$ and $n = 1$, which is identical to Fig. 9(b). Fig. 13(b) shows the amount of crustal thickening for an arc that is twice as wide. The resulting width-to-thickness ratio of 6:1 fulfils the thin sheet assumption $(\tau_{xz} \ll \tau_{xx}, \tau_{zz})$ for most materials (Artyushkov 1973). Comparing these figures, we note that the region of crustal thickening near the back of the arc persists in both figures, although this feature is shifted slightly to the north and is smaller in magnitude (as one would expect) for the wider arc. Also, a region of back-arc crustal thickening does not develop for $n = 3$ (Figs 13c and d). This qualitative test and the error analysis in Geist & Scholl (1992) indicates that large-scale features are reasonably represented using thin-sheet models with the minimum 3:1 width-to-thickness ratio.

Observations

Structural evidence indicates that deformation is nearly symmetric about the collision zone and can be categorized as compressional deformation across the arc at the latitude of collision, strike–slip faulting transverse to the arc adjacent to the zone of compressional deformation, and extensional deformation coincident with back-arc basins away from the collision zone (Fig. 3). Arcward of the d'Entrecasteaux ridge, the Maewo–Pentecost and Aoba regions are considered presently to be under compression and/or uplift (Isacks *et al.* 1981; Carney & Macfarlane 1982; Collot *et al.* 1985; Louat & Pelletier 1989), although it is debated whether Aoba Basin itself developed from recent compression associated with ridge subduction (Chung & Kanamori 1978; Collot *et al.* 1985) or was formed by an earlier episode
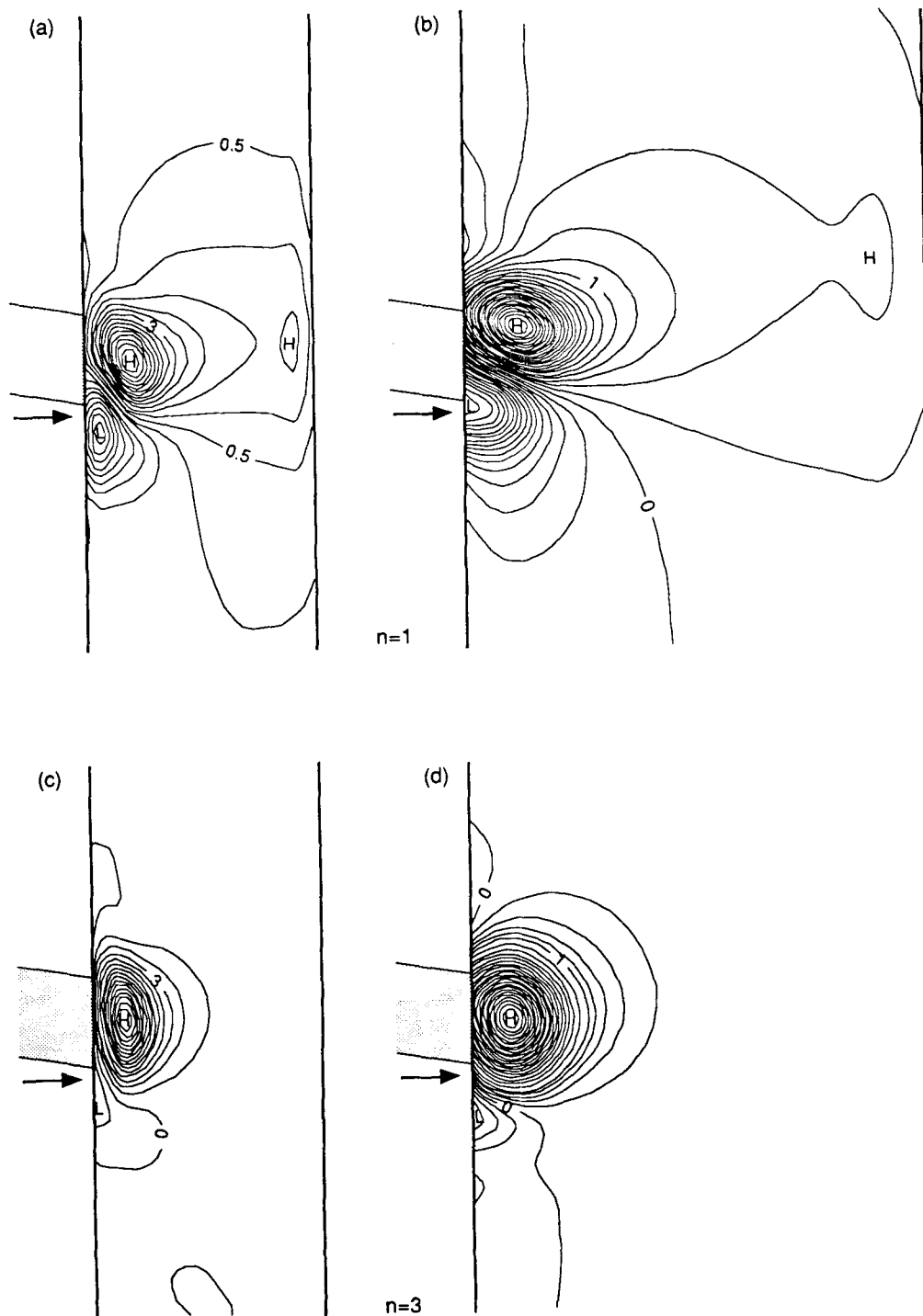
Figure 13. Qualitative test of the accuracy of using minimum thin sheet dimensions to model island arc deformation. (a) Crustal thickening due to ridge subduction in kilometres for $n = 1$ and a width-to-thickness ratio of $3:1$ (same as Fig. 9b). Contour interval is 0.5 km. (b) Same as (a) but with a width-to-thickness ratio of $6:1$. Contour interval is 0.25 km. (c and d) Same as (a) and (b) for $n = 3$.

of intra-arc rifting (Karig & Mannerickx 1972; Isacks *et al.* 1981; Marthelot *et al.* 1985; Greene *et al.* 1988). The Santo–Malekula region also has a history of reverse faulting and uplift (Taylor *et al.* 1980; Carney & Macfarlane 1982; Greene *et al.* 1988). Within and adjacent to the collision zone, transverse faulting is prevalent. For the most part, these faults are oriented E–W to NW–SE with right-lateral faulting south of the collision zone and left-lateral faulting north of the collision zone (Carney & Macfarlane 1982;

Greene *et al.* 1988). Two notable exceptions are the left-lateral Ambrym fracture zone to the south of the collision zone and the right-lateral Aoba fracture zone within the collision zone (Greene *et al.* 1988). Away from the collision zone to the north and south, young extensional back-arc troughs are presented in line with the Maweo–Pentecost ridge. To the north it is termed the Vot Tande trough and to the south it is termed the Coriolis trough by Greene *et al.* (1988).

Isacks *et al.* (1981) have provided a detailed description of the intra-arc seismicity and have classified it by regions: Santo–northern Malekula (active), southern Malekula (quiet), Efate (active) and Erromango (quiet). Within the Santo–northern Malekula segment, left-lateral events occur north-east of Espiritu Santo, whereas in the southern Malekula segment, right-lateral events (assuming the arc-normal plane as the focal plane) with a minor thrust component occur between Malekula and Efate (Fig. 3). Events with nearly vertical nodal planes are common south of Malekula and a normal faulting event near the Coriolis trough indicates that extension is presently active there. Louat & Pelletier (1989) also indicate numerous thrust faulting events distributed over 400 km along the easternmost part of the central New Hebrides arc. They also locate numerous normal faulting events coincident with the northern and southern back-arc troughs.

Most of the previously described structural features and focal mechanisms correlate with low Ar and n models (Fig. 9). The $Ar = 0$ and $n = 1$ model also predicts a high rate of crustal thickening directly arcward of the collision zone that corresponds with uplift of Espiritu Santo and a smaller ridge of uplift coincident with the Maewo–Pentecost ridge. However, the fact that crustal thinning coincident with Aoba Basin is not predicted by the models, supports a flexural origin for the basin, as described by Chung & Kanamori (1978). Higher values of n are needed to produce high shear stresses associated with transverse strike–slip faulting in the central part of the arc (Fig. 10a). Thus, these observations imply that the average value of n ranges between 1 and 3 in order to explain both the crustal thickening coincident with the Maewo–Pentecost ridge and the high shear stresses needed to initiate transverse faulting. Higher values of Ar (> 100) predict shear stresses along the edges of the arc (Fig. 11) and a small amount of crustal thickening at the collision zone, contrary to what is observed.

The high amount of rotation and crustal thinning at the frontal part of the arc in the wake of ridge subduction predicted by the $Ar = 0$ and $n = 1$ model may also explain the re-entrant structures described by Collot & Fisher (1989), who attributed these structures to subducting seamounts. Fig. 14 schematically shows the trend of normal faulting (perpendicular to the orientation of principal tensional stress) in the normal faulting zones (NS and SN). South of the ridge, the trend of normal faulting near the frontal part of the arc is curved, but not completely circular, owing to the fact that farther than 25 km away from the collision zone, the tensional stress magnitude at the arc margin is greatly diminished and probably is not sufficient to produce faulting (Figs 9a and 14). Permanent strain, recorded by the crustal thickening map (Fig. 9b), does however, reveal a roughly circular foundering of the crust with the same dimensions as the re-entrants. It is likely that the re-entrants are formed by tectonic erosion associated with subducting seamounts (Collot & Fisher 1989), augmented by stresses associated with ridge collision. Note that north of the ridge, the trend of normal faulting is nearly straight (Fig. 14) and that no crustal thinning is predicted (Fig. 9b), thus indicating that re-entrants are unlikely to form ahead of the arc–ridge collision.

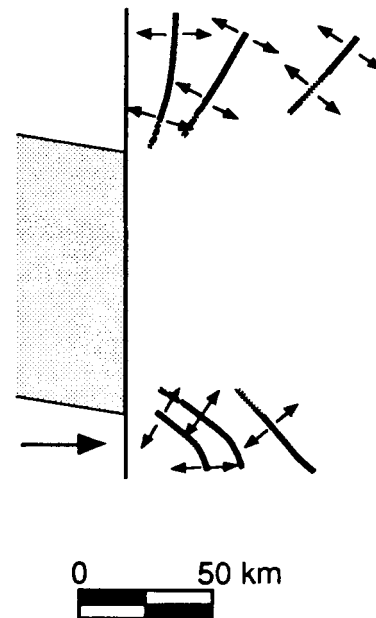The major discrepancy between deformation predicted by

Figure 14. Schematic trend of normal faults adjacent to the collision zone. Trend is determined from the normal to the principal tensional stress direction in the region where normal faulting is likely to occur (NS and SN). Within the region of secondary normal faulting (SN), the fault trend is lighter. Note that the fault trends south of the collision zone have a greater curvature than north of the collision zone. The termination of the fault trends away from the collision zone are determined by diminished magnitudes of tensional stress (Fig. 9a).

these models, to observed structure, is that back-arc extension away from the collision zone is not predicted by any of these models. This leads us to believe that the back-arc basins are formed independently from ridge subduction, similar to the formation of the Havre–Lau Basin behind the Tonga arc. The crustal thickening arcward from the collision zone (creating the Maewo–Pentecost ridge) suppresses the formation of these basins, resulting in a unique situation where compressional stress from ridge subduction is imprinted upon the tensional stress arising from back-arc spreading.

INTERPRETATION OF THIN-SHEET PARAMETERS: *Ar* AND *n*

To interpret the physical significance of the thin-sheet parameters, we estimate values for these parameters given different thermal structures and rheologies for island arcs. For a biaxial stress state, Sonder & England (1986) show that the vertically integrated strength of the lithosphere (F_L) is related to Ar by the following equation:

$$Ar = \frac{g\rho_c(1 - \rho_c/\rho_m)L^2}{F_L}. \tag{6}$$

They estimate F_L by separately estimating the upper crustal, lower crustal and mantle components F_{UC}, F_{LC} and F_M, respectively) of the vertically integrated strength. For the brittle upper crust, Sonder & England (1986) derive from

Byerlee's Law

$$F_{UC} \cong \tfrac{1}{2} z_{BD}(\sigma_1 - \sigma_3)_{BD} \quad \overline{\sigma_n} < 200 \text{ MPa}, \qquad (7)$$

where z_{BD} is the depth to the brittle–ductile transition and $\overline{\sigma_n}$ is the effective normal stress on a fault (Byerlee 1978; Brace & Kohlstedt 1980). The lower crustal component derived from the power-law relation for the high-temperature creep of quartz (England 1983; Sonder & England 1986), is

$$F_{LC} \cong \frac{\sqrt{2}^{(1/n_c-1)} T_{BD}^2 n_c R}{Q_c \gamma_c} \left(\frac{\dot{\varepsilon}}{A_c}\right)^{1/n_c} \exp\left(\frac{Q_c}{n_c R T_{BD}}\right), \qquad (8)$$

where $\dot{\varepsilon}$ is the average strain rate, T_{BD} is the absolute temperature at the brittle–ductile transition, γ_c the lower crustal geothermal gradient, R is the gas constant and A_c, n_c and Q_c are constants. Similarly, the mantle component derived from the power-law relation for the high-temperature creep of olivine (England 1983; Sonder & England 1986) is

$$F_M \cong \frac{\sqrt{2}^{1/n_p-1} T_M^2 n_p R}{Q_p \gamma_p} \left(\frac{\dot{\varepsilon}}{A_p}\right)^{1/n_p} \exp\left(\frac{Q_p}{n_p R T_M}\right), \qquad (9)$$

where T_M is the absolute temperature at the Moho, γ_p the mantle geothermal gradient, and A_p, n_p and Q_p are constants. Typical values for the constants in the power-law relation for the lower crustal and mantle rocks are given by Brace & Kohlstedt (1980), Kirby (1983) and Kirby & Kronenberg (1987).

For our calculations, we use the effective power-law exponent n (i.e. $n = n_c = n_p$) as an independent variable.

Table 1. Parameters used in calculations.

		"cold" arc	"normal" arc	"hot" arc
g	gravitational acceleration	9.8 m s⁻¹		
ρ_c	crust density	2.8 × 10³ kg m⁻³		
ρ_m	mantle density	3.3 × 10³ kg m⁻³		
L	lithosphere thickness	80 km		
T_{BD}	brittle–ductile temperature	300°C		
R	gas constant	8.314 J mol⁻¹ K⁻¹		
Q_c	activation energy for quartz power-law flow	2.19 × 10⁵ J mol⁻¹		
$\dot{\varepsilon}$	strain-rate	1.0 × 10⁻¹⁶		
A_c	constant for quartz power-law flow	5.0 × 10⁶ s⁻¹ MPa⁻ⁿ		
Q_p	activation energy for olivine power-law flow	5.2 × 10⁵ J mol⁻¹		
γ_p	mantle geotherm	15°C/km		
A_p	constant for olivine power-law flow	7.0 × 10⁴ s⁻¹ MPa⁻ⁿ		
T_M	Moho temperature	300°C	650°C	700°C-1000°C
$(\sigma_1-\sigma_3)_{BD}$	stress difference at brittle–ductile transition	240 MPa	160 MPa	120 MPa
z_{BD}	depth at brittle–ductile transition	17 km	9 km	7 km

Although n ranges between 2 and 5 for most lower crustal and mantle rocks (Kirby 1983; Kirby & Kronenberg 1987), we consider higher values to account for the steady-state sliding in the upper mantle that is neglected in eq. (9). High values of n imply perfectly plasticity (Sonder & England 1986) and that mantle and lower crustal flow is dominated by low temperature, high-stress plasticity in the upper mantle (Ashby & Verrall 1977; Tsenn & Carter 1987).

Three sets of parameters are considered for the estimation of Ar, corresponding to the rheology of (1) a 'cold' arc or forearc province, (2) a 'normal' arc, and (3) a 'hot' arc with elevated temperatures as indicated by xenolith studies (DeBari, Kay & Kay 1987) and other petrologic constraints (Tatsumi et al. 1983). The parameters in Table 1 are
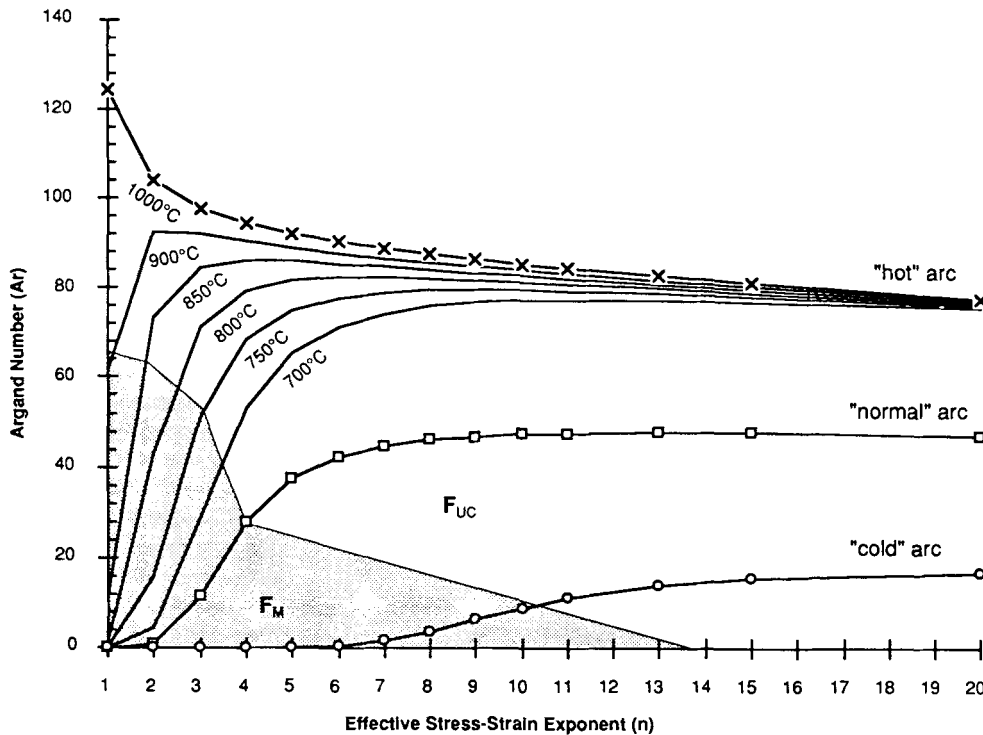

Figure 15. Effective power-law exponent (n) versus the Argand number (Ar) for three cases: (1) a 'cold' arc with depressed temperatures and increased strength, (2) a 'normal' arc, and (3) a 'hot' arc with elevated temperatures and decreased strength. For the 'hot' arc case, Moho temperatures rainging from 700°C to 1000°C are considered. Shading denotes the domain dominated by F_M in the calculation of F_L. Area without shading denotes the domain dominated by the strength of the brittle upper crust (F_{UC}).

identical for each of the three cases except for the depth and stress difference at the brittle–ductile transition and the Moho temperature. The temperature at the brittle–ductile transition is fixed at 300°C (Sibson 1984) and z_{BD} and T_M are taken from thermal models of subduction zones by Hasebe, Fujii & Uyeda (1970), Hsui & Toksöz (1979), Smirnov & Sugrobov (1980), Tatsumi et al. (1983), Cloos (1985), Honda (1985) and van den Beukel & Wortel (1988). The stress difference at the brittle–ductile transition is taken from curves published by Sibson (1984). Although the parameters listed in Table 1 are certain to have some variation, our goal is primarily to note the first-order changes in the vertically integrated strength (inverse of Ar) among the three cases.

The Argand number (Ar) plotted against the effective power-law exponent (n) (Fig. 15) shows a maximum in Ar (minimum in F_L) for the 'hot' arc case, similar to results from Sonder & England (1986). Regions where F_{UC} or F_M is the dominant component of F_L are also shown in Fig. 15. In all cases, F_{LC} is much less than F_{UC} or F_M. As expected, a thermal structure with elevated temperatures decreases the average strength of the arc, thereby increasing Ar. Deformation controlled by lower crustal and mantle flow (lower values of n) gradually gives way to deformation controlled by the upper crustal brittle regime (higher values of n). For the 'normal' and 'hot' arc cases, the gradual decreasing trend for $n > 3$ is related to the increased strength with n, i.e. increased influence of a perfect plasticity in the upper mantle. This slight decrease implies that an upper mantle layer exhibiting perfectly plastic behaviour does not contribute significantly to F_L (as also noted by Sonder & England 1986). For the 'hot' arc case, the different curves correspond to different Moho temperatures as indicated. For the 'normal' arc case, a transition from mantle-dominated flow to upper crust-dominated flow occurs at $n = 4$. For the 'cold' arc case, $Ar < 20$ for all values of n owing to the higher strength of the mantle and upper crust.

From the ridge subduction modelling performed here, low values of n and Ar conform more with the 'normal' or 'cold' arc cases. These values lie in the region dominated by mantle flow (Fig. 15) and indicate that as the strength of this layer is greater than that of the brittle upper crust, the constitutive relation for the whole lithosphere may be approximated by that of the strongest layer, namely that of a power-law rheology. This same conclusion was reached by Vilotte et al. (1982) using laboratory-derived strength profiles of Kirby (1980).

SYNTHESIS AND DISCUSSION

Arc deformation associated with ridge subduction is best modelled by low values of n and Ar, although the models are somewhat insensitive to Ar. Low values of n are implied by pervasive uplift and arc-parallel tension of the Tonga arc in the wake of Louisville ridge subduction and by crustal thickening patterns and transverse strike–slip faulting of the New Hebrides arc at the latitude of the d'Entrecasteaux collision zone. Low values of Ar are implied by the lack of high shear stress along the edges of the arcs obtained with very high Ar values. Low values of Ar indicate that the lithosphere is able to support significant crustal thickness

contrasts (Sonder et al. 1986), or as shown in the previous section that the arc is typical of a cold to normal thermal structures. However, since the duration of modelling is only over a few million years, deformation is similar for all values of $Ar < 100$, and hence, we cannot determine an absolute integrated strength of the arc lithosphere in relation to plate driving forces (e.g. McKenzie 1969; Forsyth & Uyeda 1975; Chapple & Tullis 1977; England & Wortel 1980; Turcotte 1982). In contrast, for previous continental studies the duration of modelling is tens of millions of years and most of the variation in deformation is observed for values of Ar between 0 and 30 (Sonder & England 1986).

Values of n between 1 and 3 that produce the best models for island arc deformation also differ from continental studies, where optimal values for n are greater than or equal to 3 (England & McKenzie 1982; Houseman & England 1986). Values of n less than 3 suggest that specific deformation mechanisms may affect the overall rheology of the arc lithosphere. For example, values of n are decreased in the presence of trace amounts of water. Karato, Peterson & Fitzgerald (1986) show that the power-law exponent for olivine aggregates decreases from 3.5 ± 0.7 to 3.0 ± 0.5, whereas Mackwell, Kohlstedt & Paterson (1985) suggest that $n = 2.5$ under hydrous conditions. Values of n less than 3 may indicate that a different creep regime other than power-law creep is occurring in the mantle and lower crust. For low stresses and/or very small grain size, diffusional creep (Nabarro–Herring creep or Coble creep) that is grain-size dependent obeys a Newtonian flow law (Ashby & Verrall 1977; Ranalli 1984; Ranalli & Murphy 1987; Tsenn & Carter 1987; Handy 1989). Karato et al. (1986) also show that under low strain-rates, fine-grained olivine deforms with a power-law exponent of 1.4 ± 0.3. Finally, pyroxenite has been found recently to have a stress exponent of 1.5–2.0 (Mackwell 1992) and may be important in controlling deformation in island arc regimes.

Although the material properties of the Tonga and New Hebrides arcs are similar according to the results of our models, the difference in boundary conditions produces a considerably different style of deformation. For the case where the arc–ridge intersection is quickly propagating along the plate boundary, arc-parallel tension and crustal thickening in the wake of the ridge is predicted by the models and observed along the Tonga arc. For the case where the arc–ridge intersection is stationary or slowly propagating along the plate boundary, convergence and crustal thickening directly arcward of the collision zone and transverse strike–slip faulting within and adjacent to the region arcward of the collision zone is predicted by the models and observed along the New Hebrides arc. In both cases the magnitude of stress decreases exponentially away from the collision zone and effects from ridge subduction should only be observed within 200 km of the collision zone, although once structures associated with ridge subduction are formed, they may continue to be active under the non-collisional stress regime. Also predicted in both cases is a high amount of rotation at the frontal part of the arc adjacent to the collision zone. For the Tonga case, the high amount of rotation is predicted only ahead of the ridge and corresponds to indentation and complex bathymetry of the trench slope leading the southward propagation of the ridge. For the New Hebrides case, high amounts of rotation with

opposite sense are predicted at both sides of the ridge, although crustal thinning is only predicted in the wake of the ridge. Ridge subduction thus may augment the effects of tectonic erosion to form the re-entrants described by Collot & Fisher (1989).

Isacks *et al.* (1981) pose the question whether the variations in intra-arc seismicity observed for the New Hebrides arc represents different parts of the earthquake cycle or the different ways that the arc deforms in response to ridge subduction. Results from our modelling conform more with the latter explanation, in that compressional, strike–slip and extensional deformation can all rise from the ridge subduction process alone. However, outside a range of 200 km ridge subduction should not have a significant effect on seismicity.

The results from this study can be applied to other occurrences of ridge subduction in order to examine its effect on arc deformation. For example, the Tiburon ridge is slowly converging on the Lesser Antilles arc subparallel to the orientation of the ridge and, correspondingly, the effects are similar to that of the New Hebrides arc: transverse faulting and strike–slip focal mechanisms (Stein *et al.* 1982; Bouysse & Westercamp 1990). The magnitude of deformation associated with ridge subduction is expected to be less for this case because the rate of convergence is only 20 km Myr^{-1}. In contrast, Corrigan, Mann & Ingle (1990) and Gardner *et al.* (1992) find that arc-parallel tensional stress develops from the slowly propagating Cocos ridge along the Middle America trench and attributes it to isostatic uplift from the downgoing ridge. Isostatic uplift may indeed be more important for this case, where the dip of the subducting plate is shallower (30°–45°), than for the New Hebrides, where the subducting dip is steep (70°). Transverse faulting that is also attributed to the subduction of the Cocos ridge can be related to the horizontal transmission of stress from the collision zone, as it is for the New Hebrides arc.

CONCLUSIONS

We have shown that many features associated with ridge subduction can be modelled from the horizontal transmission of stress away from the collision zone. The boundary conditions play an important role in determining the mode of deformation; this has been illustrated by analysing the extreme cases where the ridge is either propagating quickly (Tonga) or slowly (New Hebrides) along the plate boundary. Although the mode of deformation is different for the two cases, the models indicate that the physical properties are similar, such that the deformational flow is diffuse (low values of *n*) and that the lithosphere has enough vertically integrated strength to support appreciable contrasts in crustal thickness. The fact that optimal values of *n* are lower than for continental deformation may indicate that (1) water may be present in the lower crust and mantle, (2) mantle rocks obey grain-size dependent diffusional creep flow, (3) or deformation is controlled by the rheology of pyroxenite. The advantage of using the thin viscous sheet models is that lateral changes in the boundary conditions as well as a rheology similar to that which is deduced from laboratory studies can be accounted for. The fact that island arc deformation is well matched by thin viscous sheet

models illustrates the importance of the horizontal transmission of stress. This contrasts to the conclusion of Moretti & Ngokwey (1985) that because unrealistic basal shear stress (1300 MPa) from the collision process alone is required to predict uplift associated with ridge subduction, uplift is best explained by isostatic adjustments. However, the high basal shear stress they predict may be a consequence of viscoelastic modelling; for example, linearly viscous modelling of Kodama (1984) yields a maximum basal shear stress an order of magnitude less. This is not to say that isostatic effects, such as those modelled by Tomoda & Fujimoto (1983) and Moretti & Ngokwey (1985), and the mechanical wedging of the ridge, modelled by Chung & Kanamori (1978), cannot be disregarded, as they reasonably predict vertical deformation associated with ridge subduction. Specifically, it is still unresolved whether uplift associated with ridge subduction adjacent to the collision zone is a flexural (elastic) response or whether it is related to crustal thickening from the collision (plastic response). In addition to crustal thickening, thin viscous sheet modelling can predict the horizontal velocity field from which the stress regime, style of faulting and finite rotation can be obtained. Modelling of the ridge subduction process can be further improved, especially for shallow dipping subduction zones, by accounting for both the horizontal and vertical effects in a fully 3-D model using a non-linear rheology.

ACKNOWLEDGMENTS

REFERENCES

Anosov, G. I., Il'yev, A. Y., Suvorov, A. A., Argentov, V. V., Neverov, Y. A., Zhil'tsov, E. G., & Patrikeyev, V. N., 1983. Features of the geological structure of the junction zone between the Tonga and Kermadec trenches, *Geotectonics*, **17**, 252–261.

Artyushkov, E. V., 1973. Stresses in the lithosphere caused by crustal thickness inhomogeneities, *J. geophys. Res.*, **78**, 7675–7708.

Ashby, M. F. & Verrall, R. A., 1977. Micromechanisms of flow and fracture, and their relevance to the rheology of the upper mantle, *Phil. Trans. R. Soc. Lond., A*, **288**, 59–95.

Austin, J. A., Jr, Taylor, F. W. & Cagle, C. D., 1989. Seismic stratigraphy of the central Tonga Ridge, *Mar. Petrol. Geol.*, **6**, 71–92.

Ballance, P. F., Scholl, D. W., Vallier, T. L., Stevenson, A. J., Ryan, H. & Herzer, R. H., 1989. Subduction of a Late Cretaceous seamount of the Louisville ridge at the Tonga trench: a model of normal and accelerated tectonic erosion, *Tectonics*, **8**, 953–962.

Bird, P., 1978. Stress and temperature in subduction shear zones: Tonga and Mariana, *Geophys J. R. astr. Soc.*, **55**, 411–434.

Bird, P., 1989. New finite element techniques for modeling deformation histories of continents with stratified temperature-dependent rheology, *J. geophys. Res.*, **94**, 3967–3990.

Bouysse, P. & Westercamp, D., 1990. Subduction of Atlantic aseismic ridges and Late Cenozoic evolution of the Lesser Antilles island arc, *Tectonophysics*, **175**, 349–380.

Brace, W. F. & Kohlstedt, D. L., 1980. Limits on lithospheric stress imposed by laboratory experiments, *J. geophys. Res.*, **85**, 6248–6252.

Burne, R. V., Collot, J. Y. & Daniel, J., 1988. Superficial structures and stress regimes of the downgoing plate associated with subduction-collision in the central New Hebrides arc (Vanuatu), in *Geology and Offshore Resources of Pacific Island Arcs—Vanuatu Region*, pp. 357–376, eds Greene, H. G. & Wong, F. L., Circum-Pacific Council for Energy and Mineral Resources, Earth Science Series, 8.

Byerlee, J., 1978. Friction in rocks, *Pure appl. Geophys.*, **116**, 615–626.

Carney, J. N. & Macfarlane, A., 1982. Geological evidence bearing on the Miocene to Recent structural evolution of the New Hebrides arc, *Tectonophysics*, **87**, 147–175.

Chapple, W. M. & Tullis, T. E., 1977. Evolution of the forces that drive the plates, *J. geophys. Res.*, **82**, 1967–1984.

Chatelain, J. L. & Grasso, J. R., 1992. Spatial and temporal seismic energy release in the Efate region (central New Hebrides island arc): evidence for buckling?, *Geophys. Res. Lett.*, **19**, 1157–1160.

Christensen, D. H. & Lay, T., 1988. Large earthquakes in the Tonga region associated with subduction of the Louisville ridge, *J. geophys. Res.*, **93**, 13367–13389.

Chung, W. Y. & Kanamori, H., 1978. A mechanical model for plate deformation associated wtih aseismic ridge subduction in the New Hebrides arc, *Tectonophysics*, **50**, 29–40.

Cloos, M., 1985. Thermal evolution of convergent plate margins: thermal modeling and re-evaluation of istopic Ar-ages for blueschists in the Franciscan complex of California, *Tectonics*, **4**, 421–433.

Collot, J. Y. & Fisher, M. A., 1989. Formation of forearc basins by collision between seamounts and accretionary wedges: an example from the New Hebrides subduction zone, *Geology*, **17**, 930–933.

Collot, J. Y. & Fisher, M. A., 1991. The collision zone between the north d'Entrecasteaux ridge and the New Hebrides island arc 1. Sea Beam morphology and shallow structure, *J. geophys. Res.*, **96**, 4457–4478.

Collot, J. Y. & Malahoff, A., 1982. Anomalies gravimétriques et structure de la zone de subduction des Nouvelles-Hébrides, in *Contribution à l'étude géodynamique du Sud-Ouest Pacifique*, pp. 91–109 Travaux et Documents de l'ORSTOM, no. 147.

Collot, J. Y., Daniel, J. & Burne, R. V., 1985. Recent tectonics associated with the subduction/collision of the d'Entrecasteaux zone in the central New Hebrides, *Tectonophysics*, **112**, 325–356.

Corrigan, J., Mann, P. & Ingle, J. C., 1990. Forearc response to subduction of the Cocos Ridge, Panama–Costa Rica, *Geol. Soc. Am. Bull.*, **102**, 628–652.

Davies, G. F., 1981. Regional compensation of subducted lithosphere: effects on geoid, gravity and topography from a preliminary model, *Earth planet. Sci. Lett.*, **54**, 431–441.

DeBari, S., Kay, S. M. & Kay, R. W., 1987. Ultramafic xenoliths from Adagdak Volcano, Adak, Aleutian Islands, Alaska: deformed igneous cumulates from the Moho of an island arc, *J. Geol.*, **95**, 329–341.

Dupont, J. & Herzer, R. H., 1985. Effect of subduction of the Louisville ridge on the structure and morphology of the Tonga arc, in *Geology and Offshore Resources of Pacific Island Arcs—Tonga Region*, pp. 323–332, eds Scholl, D. W. & Vallier, T. L., Circum-Pacific Council for Energy and Mineral Resources, Earth Science Series, 2.

England, P. C., 1982. Some numerical investigations of large scale continental deformation, in *Mountain Building Processes*, pp. 129–139, ed. Hsü, K. J., Academic Press, London.

England, P. C., 1983. Constraints on extension of continental lithosphere, *J. geophys. Res.*, **88**, 1145–1152.

England, P. C. & McKenzie, D. P., 1982. A thin viscous sheet model for continental deformation, *Geophys. J. R. astr. Soc.*, **70**, 295–321.

England, P. C. & McKenzie, D. P., 1983. Correction to: a thin viscous sheet model for continental deformation, *Geophys. J. R. astr. Soc*, **73**, 523–532.

England, P. C. & Wortel, R., 1980. Some consequences of the subduction of young slabs, *Earth planet. Sci. Lett.*, **47**, 403–415.

Fisher, M. A., 1986. Tectonic processes at the collision of the d'Entrecasteaux zone and the New Hebrides island arc, *J. geophys. Res.*, **91**, 10470–10486.

Fisher, M. A., Collot, J. Y. & Smith, G. L., 1986. Possible causes for structural variation where the New Hebrides island arc and the d'Entrecasteaux zone collide, *Geology*, **14**, 951–954.

Fisher, M. A., Collot, J. Y. & Geist, E. L., 1991. The collision zone between the north d'Entrecasteaux ridge and the New Hebrides island arc 2. Structure from multichannel seismic data, *J. geophys. Res.*, **96**, 4479–4495.

Forsyth, D. W., 1980. Comparison of mechanical models of the oceanic lithosphere, *J. Geophys. Res.*, **85**, 6364–6368.

Forsyth, D. W. & Uyeda, S., 1975. On the relative importance of the driving forces of plate motion, *Geophys. J. R. astr. Soc.*, **105**, 163–200.

Fleitout, L. & Froidevaux, C., 1982. Tectonics and topography for a lithosphere containing density heterogeneities, *Tectonics*, **1**, 21–56.

Fryer, P. & Smoot, N. C., 1985. Processes of seamount subduction in the Mariana and Izu–Bonin trenches, *Mar. Geol.*, **64**, 77–90.

Gardner, T. W., Verdonck, D., Pinter, N. M., Slingerland, R., Furlong, K. P., Bullard, T. F. & Wells, S. G., 1992. Quaternary uplift astride the aseismic Cocos Ridge, Pacific coast, Costa Rica, *Geol. Soc. Am. Bull.*, **104**, 219–232.

Geist, E. L. & Scholl, D. W., 1992. Application of continuum models to deformation of the Aleutian island arc, *J. geophys. Res.*, **97**, 4953–4967.

Gnibidenko, H. S., Anosov, G. I., Argentov, V. V. & Pushchin, I. K., 1985. Tectonics of the Tonga–Kermadec trench and Ozbourn Seamount junction area, *Tectonophysics*, **112**, 357–383.

Goetze, C., 1978. The mechanisms of creep in olivine, *Phil. Trans. R. Soc. Lond.*, A, **288**, 99–119.

Greene, H. G., Macfarlane, A., Johnson, D. P. & Crawford, A., 1988. Structure and tectonics of the central New Hebrides arc, in *Geology and Offshore Resources of Pacific Island Arcs—Vanuatu Region*, pp. 377–412, eds Greene, H. G. & Wong, F. L., Circum-Pacific Council for Energy and Mineral Resources, Earth Science Series, 8.

Grow, J. A., 1973. Crustal and upper mantle structure of the central Aleutian Arc, *Geol. Soc. Am. Bull.*, **84**, 2169–2192.

Handy, M. R., 1989. Deformation regimes and the rheological evolution of fault zones in the lithosphere: the effects of pressure, temperature, grainsize and time, *Tectonophysics*, **163**, 119–152.

Hasebe, K., Fujii, N. & Uyeda, S., 1970. Thermal processes under island arcs, *Tectonophysics*, **10**, 335–355.

Herzer, R. H. & Exon, N. F., 1985. Structure and basin analysis of the southern Tonga forearc, in *Geology and Offshore Resources of Pacific Island Arcs—Tonga Region*, pp. 55–73, eds Scholl, D. W. & Vallier, T. L., Circum-Pacific Council for Energy and Mineral Resources, Earth Science Series, 2.

Honda, S., 1985. Thermal structure beneath Tohoku, northeast Japan—a case study for understanding the detailed thermal structure of the subduction zone, *Tectonophysics*, **112**, 69–102.

Houseman, G. A. & England, P. C., 1986. Finite strain calculations of continental deformation 1. Method and general results for convergent zones, *J. geophys. Res.*, **91**, 3651–3663.

Hsui, A. T. & Toksöz, M. N., 1979. The evolution of thermal structures beneath a subduction zone, *Tectonophysics*, **60**, 43–60.

Isacks, B. L., Cardwell, R. K., Chatelain, J. L., Barazangi, M., Marthelot, J. M., Chinn, D. & Louat, R., 1981. Seismicity and tectonics of the central New Hebrides island arc, in *Earthquake Prediction: an International Review*, pp. 93–116, eds Simpson, D. W. & Richards, P. G., *Am. geophys. Union, Maurice Ewing Ser.*, **4**.

Karato, S. I., Paterson, M. S. & Fitzgerald, J. D., 1986. Rheology of synthetic olivine aggregates: influence of grain size and water, *J. geophys. Res.*, **91**, 8151–8176.

Karig, D. E. & Mammerickx, J., 1972. Tectonic framework of the New Hebrides island arc, *Mar. Geol.*, **12**, 187–205.

Kirby, S. H., 1980. Tectonic stresses in the lithosphere: constraints provided by the experimental deformation of rocks, *J. geophys. Res.*, **85**, 6353–6363.

Kirby, S. H., 1983. Rheology of the lithosphere, *Rev. Geophys. Space Phys.*, **21**, 1458–1487.

Kirby, S. H. & Kronenberg, A. K., 1987. Rheology of the lithosphere: selected topics, *Rev. Geophys.*, **25**, 1219–1244.

Kodama, K., 1984. A simple model calculation of the shear stress and surface profile caused by the perturbation on subducting plate, *Zisin, J. seism. Soc. Jpn*, **37**, 647–654.

Lallemand, S. E. & Le Pichon, X., 1987. Coulomb wedge model applied to the subduction of seamounts in the Japan trench, *Geology*, **15**, 1065–1069.

Lallemand, S. E., Malavieille, J. & Calassou, S., 1992. Effects of oceanic ridge subduction on accretionary wedges: experimenal modeling and marine observations, *Tectonics*, **11**, 1301–1313.

Lonsdale, P., 1986. A multibeam reconnaissance of the Tonga trench axis and its intersection with the Louisville guyot chain, *Mar. geophys. Res.*, **8**, 295–327.

Louat, R. & Pelletier, B., 1989. Seismotectonics and present-day relative plate motions in the New Hebrides–North Fiji Basin region, *Tectonophysics*, **167**, 41–55.

Louat, R., Hamburger, M. & Monzier, M., 1988. Shallow and intermediate depth seismicity in the New Hebrides arc: constraints on the subduction process, in *Geology and Offshore Resources of Pacific Island Arcs—Vanuatu Region*, pp. 329–356, eds Greene, H. G. & Wong, F. L., Circum-Pacific Council for Energy and Mineral Resources, Earth Science Series, 8.

Macharé, J. & Ortlieb, L., 1992. Plio-Quaternary vertical motions and the subduction of the Nazca Ridge, central coast of Peru, *Tectonophysics*, **205**, 97–108.

Mackwell, S. J., 1992. Deformation of fine-grained pyroxenite: application to lithosphere dynamics, *EOS, Trans. Am. geophys. Un.*, **73** (supplement), 528.

Mackwell, S. J., Kohlstedt, D. L. & Paterson, M. S., 1985. The role of water in the deformation of olivine single crystals. *J. geophys. Res.*, **90**, 11319–11333.

Marthelot, J. M., Chatelain, J. L., Isacks, B. L., Cardwell, R. K. & Coudert, E., 1985. Seismicity and attenuation in the central Vanuatu (New Hebrides) Islands: a new interpretation of the effect of subduction of the d'Entrecasteaux fracture zone, *J. geophys. Res.*, **90**, 8641–8650.

McCann, W. R. & Habermann, R. E., 1989. Morphologic and geologic effects of the subduction of bathymetric highs, *Pure appl. Geophys.*, **129**, 41–69.

McKenzie, D. P., 1969. Speculations on the consequences and causes of plate motions, *Geophys. J. R. astr. Soc.*, **18**, 1–32.

McKenzie, D. P. & Jackson, J. A., 1983. The relationship between strain rates, crustal thickening, paleomagnetism, finite strain and fault movements within a deforming zone, *Earth planet. Sci. Lett.*, **65**, 182–202.

Melosh, H. J. & Raefsky, A., 1980. The dynamical origin of

subduction zone topography, *Geophys. J. R. astr. Soc*, **60**, 333–354.

Minster, J. B. & Jordan, T. H., 1978. Present day plate motions, *J. geophys. Res.*, **83**, 5331–5354.

Moretti, I. & Ngokwey, K., 1985. Aseismic ridge subduction and vertical motion of overriding plate, in *Caribbean Geodynamics*, pp. 245–253, ed. Mascle, A., Symposium sur la Géodynamique des Caraibes.

Pelletier, B. & Dupont, J., 1990. Effects de la subduction de la ride de Louisville sur l'arc des Tonga–Kermadec, *Oceanol. Acta*, **10**, 57–76.

Pelletier, B. & Louat, R., 1989. Seismotectonics and present-day relative plate motions in the Tonga–Lau and Kermadec–Havre region, *Tectonophysics*, **165**, 237–250.

Pontoise, B. & Latham, G., 1982. Étude par réfraction de la structure interne de l'arc des Tonga, in *Contribution à l'étude géodynamique de Sud-Quest Pacifique*, pp. 283–291. Travaux et Documents de l'ORSTOM, no. 147.

Pontoise, B., Latham, G. & Ibrahim, A. K., 1982. Sismique réfraction: structure de la croute aux Nouvelles-Hébrides, in *Contribution à l'étude géodynamique du Sud-Ouest Pacifique*, pp. 283–291, Travaux et Documents de l'ORSTOM, no. 147.

Ranalli, G., 1984. On the possibility of Newtonian flow in the upper mantle, *Tectonophysics*, **108**, 179–192.

Ranalli, G. & Murphy, D. C., 1987. Rheological stratification of the lithosphere, *Tectonophysics*, **132**, 281–295.

Sato, T. & Matsu'ura, M., 1988. A kinematic model for deformation of the lithosphere at subduction zones, *J. geophys. Res.*, **93**, 6410–6418.

Shemenda, A. I., 1992. Horizontal lithosphere compression and subduction: constraints provided by physical modeling, *J. geophys. Res.*, **97**, 11097–11116.

Sibson, R. H., 1984. Roughness at the base of the seismogenic zone: contributing factors. *J. geophys. Res.*, **89**, 5791–5799.

Sleep, N. H., 1975. Stress and flow beneath island arcs, *Geophys. J. R. astr. Soc.*, **42**, 827–857.

Smirnov, Y. B. & Sugrobov, V. M., 1980. Terrestrial heat flow in the Kurile–Kamchatka and Aleutian provinces. III. Assessments of temperature at depth and thickness of the lithosphere, *Volc. Seism.*, **2**, 3–18.

Sonder, L. J. & England, P. C., 1986. Vertical averages of rheology of the continental lithosphere: relation to thin sheet parameters, *Earth planet. Sci. Lett.*, **77**, 81–90.

Sonder, L. J., England, P. C. & Houseman, G. A., 1986. Continuum calculations of continental deformation in transcurrent environments, *J. geophys. Res.*, **91**, 4797–4810.

Stein, S., Engeln, J. F., Wiens, D. A., Fujita, K. & Speed, R. C., 1982. Subduction seismicity and tectonics in the Lesser Antilles arc, *J. geophys. Res.*, **87**, 8642–8664.

Tapponier, P. & Molnar, P., 1976. Slip-line field theory and large-scale continental tectonics, *Nature*, **264**, 319–324.

Tatsumi, Y., Sakuyama, M., Fukuyama, H. & Kushiro, I., 1983. Generation of arc basalt magmas and thermal structure of the mantle wedge in subduction zones, *J. geophys. Res.*, **88**, 5815–5825.

Taylor, F. W., 1978. Quarternary tectonic and sea-level history, Tonga and Fiji, southwest Pacific, *PhD Thesis*, Cornell University, University Microfilms International, Ann Arbor, MI.

Taylor, F. W., Isacks, B. L., Jouannic, C., Bloom, A. L. & Dubois, J., 1980. Coseismic and Quaternary vertical tectonic movements, Santo and Malekula Islands, New Hebrides island arc, *J. geophys. Res.*, **85**, 5367–5381.

Tharp, T. M., 1985. Numerical models of subduction and forearc deformation, *Geophys. J. R. astr. Soc*, **80**, 419–437.

Tomoda, Y. & Fujimoto, H., 1983. Roles of seamount, rise, and ridge in lithospheric subduction, in *Accretion Tectonics in the*

circum-Pacific Regions, pp. 319–331, eds Hashimoto, M. & Uyeda, S, Terra Scientific Publishing Company, Tokyo.

Tsenn, M. C. & Carter, N. L., 1987. Upper limits of power law creep of rocks, *Tectonophysics*, **136**, 1–26.

Turcotte, D. L., 1982. Driving mechanisms of mountain building, in *Mountain Building Processes*, pp. 141–146, ed. Hsü, K. J., Academic Press, London.

Turcotte, D. L. & Schubert, G., 1982. *Geodynamics: Applications of Continuum Physics to Geological Problems*, Wiley, New York.

Vilotte, J. P., Daignières, M. & Madariaga, R., 1982. Numerical modeling of intraplate deformation: simple mechanical models of continental collision, *J. geophys. Res.*, **87**, 10709–10728.

Van den Beukel, J. & Wortel, R., 1988. Thermo-mechanical modeling of arc-trench regions, *Tectonophysics*, **154**, 177–193.

Von Huene, R., Suess, E. & Leg 112 Shipboard Scientists, 1988. Ocean Drilling Programs Leg 112, Peru continental margin: Part 1, tectonic history, *Geology*, **16**, 934–938.

Walcott, R. I., 1970. Flexural rigidity, thickness, and viscosity of the lithosphere, *J. geophys. Res.*, **75**, 3941–3954.

Wdowinski, S., 1992. Dynamically supported trench topography, *J. geophys. Res.*, **97**, 17651–17656.

Wdowinski, S. & O'Connell, R. J., 1990. On the choice of boundary conditions in continuum models of continental deformation, *Geophys. Res. Lett.*, **17**, 2413–2416.

Yang, C. S., Segawa, J. & Fukuda, Y., 1992. Density structure of the Mariana Arc and its vicinity obtained from successive inversion of the gravity anomaly, *Tectonophysics*, **206**, 325–339.

Zhang, J., Hager, B. H. & Raefsky, A., 1985. A critical assessment of viscous models of trench topography and corner flow, *Geophys. J. R. astr. Soc.*, **83**, 451–475.

Zhong, S. & Gurnis, M., 1992. Viscous flow model of a subduction zone with a faulted lithosphere: long and short wavelength topography, gravity, and geoid, *Geophys. Res. Lett.*, **19**, 1891–1894.

APPENDIX

Departure from the assumptions used in thin viscous sheet modelling caused by vertical traction at the subduction zone boundary can be estimated if the lateral variation of vertical shear stress (τ_{xz}) is known. Dynamic support at the trench is important with respect to thin viscous sheet modelling in that the vertical shear stress is assumed to be zero. Because the dip of the subducted slab is steep for the Tonga and New Hebrides subduction zones, vertical deformation of the island arc can be approximated by a vertical end-load. Assume that the vertical shear stress (τ_{xz}) varies away from the trench according to

$$\tau_{xz} = -T_{xz}f(x), \qquad (A1)$$

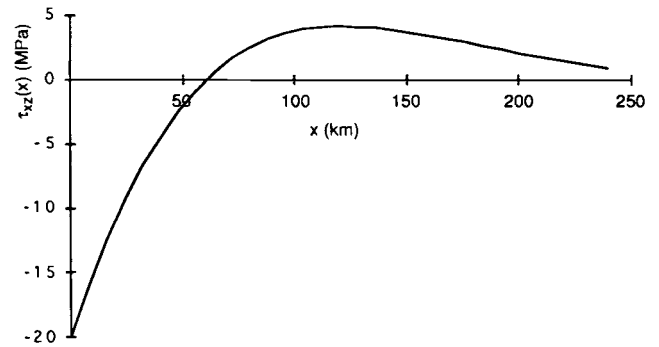where T_{xz} is the constant vertical shear traction at the

Figure A1. Vertical shear stress (τ_{xz}) associated with vertical shear traction applied at the trench ($x = 0$). Curve derived from the expressions of elastic flexure (Chung & Kanamori 1978; Turcotte & Schubert 1982). Thin viscous sheet models assume τ_{xz} is zero and thus are least accurate near the trench. The maximum positive shear stress at $x = 120$ km is approximately 15 per cent of the average principal stress predicted by the thin viscous sheet models.

boundary and $f(x)$ is a differentiable function. We use a form of $f(x)$ from expressions describing simple elastic flexure of the lithosphere. In this case, shear stress varies as the third derivative of the deflection such that

$$\tau_{xz} = c_1 \frac{d^3w}{dx^3}. \qquad (A2)$$

The constant c_1 is dependent on Young's modulus and Poisson's ratio. The deflection (w) is given by Turcotte & Schubert (1982):

$$w(x) = w_0 e^{-x/\alpha} \cos(x/\alpha), \qquad (A3)$$

where

$$\alpha = \left[\frac{4D}{(\rho_m - \rho_w)g} \right]^{1/4} \qquad (A4)$$

and where D is the flexural rigidity, and ρ_w and ρ_m are water and mantle densities, respectively. Rather than using estimates of the material constants for determining c_1, we will let $\tau_{xz}(x = 0) = -T_{xz}$ so that

$$\tau_{xz} = -T_{xz} e^{-x/\alpha} [\cos(x/\alpha) - \sin(x/\alpha)]. \qquad (A5)$$

Fig. A1 shows the variaton of τ_{xz} with x using a flexural rigidity of 2×10^{23} N m (Walcott 1970) and 20 MPa shear traction at the trench (T_{xz}) (Bird 1978). Away from the trench, the maximum shear stress occurring at 120 km is approximately 4 MPa or 15 per cent of the average magnitude of stress near the collision zone from thin viscous sheet modelling of ridge subduction.